Polar or not polar? The interplay between reconstruction, Sr enrichment, and reduction at the La0.75Sr0.25MnO3 (001) surface

Editors' Suggestion

Polar or not polar? The interplay between reconstruction, Sr enrichment, and reduction at the $La_{0.75}Sr_{0.25}MnO_3$ (001) surface

Franziska Hess[1] and Bilge Yildiz[1,2,*]

[1]*Department of Nuclear Science and Engineering, 77 Massachusetts Avenue, Massachusetts Institute of Technology Cambridge, Massachusetts 02139, USA*

[2]*Department of Materials Science and Engineering, 77 Massachusetts Avenue, Massachusetts Institute of Technology Cambridge, Massachusetts 02139, USA*

(Received 2 October 2019; published 31 January 2020)

Perovskite oxides used in heterogeneous catalysis and electrocatalysis are tuned by substitutional doping. Sr-doped $LaMnO_3$ is a popular choice of electrode material for electrochemical energy conversion. At elevated temperatures, relevant to solid oxide fuel or electrolysis cells, Sr enriches at the surface, which leads to fast degradation of the oxygen exchange activity at the surface. In this work, we investigate the effect of oxygen partial pressure $p(O_2)$ and temperature on Sr segregation at the $La_{0.75}Sr_{0.25}MnO_3(001)$ (LSM25) surface by *ab initio* thermodynamics calculations, taking into account different terminations and point defects Sr'_{La}, $V^{\cdot\cdot}_{O}$, V'''_{Mn}, V'''_{La}, O_{ad}, as well as associated defects of the type $[V^{\cdot\cdot}_{O} - V'''_{cation}]$. This model of the LSM25(001) surface addresses the connection between point defects and surface stability and makes quantitative predictions about the surface termination and Sr enrichment. Our results indicate that the MnO_2 termination is stable under oxidizing conditions, while a partially covering SrO termination on MnO_2 is stable for reaction conditions between 1000 and 1400 K and effective oxygen partial pressures between 10^{-11} bar and 0.1 bar relevant to solid oxide fuel cell (SOFC) cathodes. Under more reducing conditions, we find that Sr is enriched at the surface regardless of surface termination. This trend is a direct consequence of the increased formation of positively charged oxygen vacancies at the surface, and this conclusion holds regardless of which surface termination is assumed. The partial SrO termination is exceptionally stable under SOFC cathode conditions because it minimizes the surface dipole density, while all the defect-free terminations of LSM25(001) are unstable due to surface polarity. This newly proposed termination leaves both Sr, as well as Mn and O sites of the MnO_2 layer exposed at the surface and available for interaction with the gas phase. We propose that the LSM25(001) surface may consist of coexisting (La,Sr)O and MnO_2 domains under SOFC cathode conditions, and we propose to include such a micropatterned surface in the future discussion of the active site in the oxygen reduction reaction.

DOI: 10.1103/PhysRevMaterials.4.015801

I. INTRODUCTION

Perovskite oxides are a flexible class of materials whose properties can be tuned by chemical doping to make them suitable for a wide variety of applications. Their chemical and electrochemical applications range from heterogeneous catalysis [1–3] and solar-to-fuels [4–6], to oxide ion [7] or proton conductors [7,8], electrode materials [2,9,10], and ferroelectronics [11–16]. Their general composition can be expressed as ABO_3, where A and B represent a large and a small cation, respectively. They are very tolerant toward substitution on either site, which enables tuning their properties to the application and creates materials with rich defect chemistry. This makes them a real "playground" for theory and materials design [17].

Mixed ionic and electronic conductors (MIECs) from the perovskite family, such as $La_{1-x}Sr_xMnO_{3+\delta}$ (LSM), $La_{1-x}Sr_xCoO_{3+\delta}$ (LSC) or $La_{1-x}Sr_xCo_{1-y}Fe_yO_{3+\delta}$ (LSCF) are popular materials used as solid oxide fuel cell (SOFC) cathodes due to their high activity for the oxygen reduction reaction (ORR) and high ionic and electronic conductivity. Although the bulk electronic and ionic properties of these materials are well-understood [2,9,18–20], the surface properties are not [17]. The surface structure and composition change dynamically with temperature, oxygen partial pressure and polarization. This often leads to significant deviations from the bulk properties in the boundary region close to the surface after being subjected to elevated temperatures [10,21–28].

Both in catalytic and electrocatalytic applications, the surface termination plays a crucial role for the surface-gas interaction. The A-site cation(s), which are typically from the earth alkali or rare earth groups have fundamentally different properties than the B-site cations, which are transition metal elements. In catalysis, these different properties give rise to interesting applications that combine redox (transition metal) with acid-base (earth alkali metal) catalysis [3]. The undercoordinated transition metal sites are regarded as vital in the oxygen reduction reaction (ORR) [29–34], even though the A site (earth alkali/rare earth) may also be active in catalyzing the ORR [29,30,35,36]. While there is currently no clear answer regarding the active site in the ORR on perovskite oxides,

*Corresponding author: byildiz@mit.edu

including LSM, the surface structure and composition likely plays a major role in determining the activity of ORR [37]. Tailoring the surface properties of these materials, however, is a major challenge that can be overcome only with more understanding of how their surfaces respond to stimuli from the environment.

In Sr-doped perovskites for SOFC and related applications, such as $La_{1-x}Sr_xMnO_{3+\delta}$, the deviation of the surface composition from the bulk, dubbed surface segregation, typically involves a change both in the composition and the phase near the surface. Specifically this process can lead to the enrichment of Sr cations close to the surface [21,38–42], and also to the formation of Sr-enriched secondary phase precipitates at the surface that are electronically and ionically insulating [23]. These surface layers and precipitates severely impede the oxygen exchange at the surface, thus leading to degradation of the electrode [26,43,44].

Similar effects have been observed in a large variety of perovskite materials and for other dopant cations [21,22]. The overview of materials in Ref. [21] shows that this phenomenon is not unique to a particular material or a particular element. Rather, the enrichment of particular (A, A', B, B') cations under different thermodynamic conditions may be considered as an intrinsic property of many (if not all) perovskite.

Dopant segregation in SOFC cathode materials has been studied by a variety of experimental and theoretical methods, which have been reviewed recently [21,22]. Theoretical studies attempting to explain Sr segregation have approached the problem on fundamental levels and have drawn four major conclusions as will be summarized in the following.

First, the cation size mismatch between host and dopant cations has been successfully linked to the observed and computed segregation [24,41,45,46], with larger dopant cations segregating more and segregation onset at lower temperatures. This aspect of segregation is quite well-understood at this point. However, it is not able to explain the segregation of A-site cations in undoped perovskite materials.

Second, perovskite oxide surfaces and interfaces suffer from the fundamental problem of surface polarity. This becomes evident if one considers the stacking of AO and BO_2 layers in [001] direction. Cleaving the surface leads to either AO or BO_2 termination. If both A and B cations have a $+3$ charge, these AO and BO_2 layers have $+1$ and -1 net charge, respectively. Cleaving the structure thus creates dipolar surfaces of Tasker type 3 with diverging surface energy [47]. These types of surfaces cannot be stable without undergoing significant charge rearrangement, defect segregation or surface reconstruction [48]. However, even if A- and B-site cations have oxidation states $+2$ and $+4$ and one would expect the AO and BO_2 layers to be formally neutral, the surfaces can be weakly polar (as is the case for $SrTiO_3$) [49]. This is because the net charges of "Sr^{2+}" and "O^{2-}" in $SrTiO_3$ are not equivalent due to covalent electron sharing between O and Ti. As a consequence, even surfaces that appear neutral when assuming formal charges may actually be polar. As a result, such polarity induces segregation of charged defects or surface reconstruction, such as the enrichment of Sr or other charged point defects close to charged surface terminations [23,42,50].

Third is the coupling of Sr concentration to the oxygen nonstoichiometry. It must be noted that the materials used as SOFC electrodes are oxygen-nonstoichiometric. They support a high concentration of oxygen vacancies (under reducing conditions) or cation vacancies (under oxidizing conditions). Under SOFC operating conditions (high temperature, cathodic potential) the surface is assumed to be enriched in oxygen vacancies [24–26,51] with positive formal charge, as it has also been observed at surfaces and interfaces of binary oxides, such as doped CeO_2 [52–57] and ZrO_2 [53,58]. Accumulation and ordering of such defects have been shown to induce surface reconstructions in $TiO_2(110)$ [59]. These charged defects can attract aliovalently doped cations, such as Sr^{2+} in LSM, to the surface [24,60]. Evidently, the opposite is true, i.e., the presence of Sr close to the surface stabilizes oxygen vacancies, and links Sr near-surface enrichment to oxygen deficiency.

And fourth, even without considering oxygen vacancies, surface reduction is able to explain the preference of the AO termination over the BO_2 termination. This is due to the fact that the AO termination is less oxygen-rich, which makes it favored over the BO_2 termination under reducing conditions, as shown for $LaMnO_3$ in an *ab initio* thermodynamics model [61]. Partial substitution of La by Sr in the termination layer moves the thermodynamic transition boundary between the MnO_2- and (La,Sr)O termination to less reducing conditions. This makes a partially Sr-substituted AO termination the stable surface under SOFC conditions, which also explains the fact that Sr is enriched at the surface under SOFC operating conditions [61].

All the previous studies are limited to the examination of one particular driving force of Sr segregation at a time, neglecting other factors. For instance, the study of Y.-L. Lee and Morgan investigates only the polarity of defect-free terminations and how it interacts with given charged defects, but does not consider which of these defects are thermodynamically stable [62]. Sharma *et al.* examine how surface oxygen vacancies attract Sr to the AO-terminated surface and their thermodynamic stability under reducing conditions but do not consider other terminations or charged defects, such as negatively charged cation vacancies, which should be by far more stable at the positively charged AO termination [60]. W. Lee *et al.* and Harrison study specifically the interaction of different charged defects at the BO_2 and AO terminations, but do not consider thermodynamic stabilities of these structures or other terminations [42,50]. Finally, Piskunov *et al.* study the thermodynamics of different LSM terminations in a rigorous manner, but limit their considerations to defect-free surface structures [61]. As shown in a number of experimental studies, the perovskite (001) surfaces are often not bulk-terminated, showing a variety of reconstructions [63–67] and compositional changes after annealing [40,68,69]. We therefore propose that surface termination, defect concentration and dopant enrichment are not independent of each other and must be studied collectively.

In this manuscript, our key contribution is the *ab initio* thermodynamic assessment of the surface segregation phenomenon by simultaneously taking into account the thermodynamic stability of different terminations with a variety of point defects. The terminations and point defects are connected to Sr enrichment close to the surface, spanning a wide range of temperatures and oxygen partial pressures. We

show that considering collectively the surface termination, point defects and Sr enrichment is crucial in predicting the surface structure and composition. We further propose that the association of cation and oxygen vacancies at the surface gives the surface additional degrees of freedom to reduce the surface free energy. This gives rise to a new type of surface termination where AO and BO_2 domains coexist at the surface, thereby minimizing the surface dipole moment. Such a "partial" termination where all A sites are occupied by Sr is found to be exceptionally stable under reducing conditions relevant to ORR. Further enrichment of Sr near the surface as the gas phase becomes more reducing is driven by electrostatic attraction of positively charged surface oxygen vacancies and the negatively charged Sr dopant.

Our *ab initio* thermodynamics model is able to quantitatively predict the composition and structure of the near-surface region under given temperature and $p(O_2)$ for a non-stoichiometric oxide with rich defect chemistry and complex surface structure. We can identify three regimes of $(T, p(O_2))$ where the surface exhibits different features and gain a deeper understanding of what drives these surface changes. Beside our new insight into Sr segregation, we propose that such a model would also be useful for other complex nonstoichiometric oxides [70] employed in catalysis to predict surface structure of complex catalyst materials under operating conditions.

II. COMPUTATIONAL DETAILS

To study segregation, we represent the surface in the form of a symmetric slab and the bulk in the form of a bulk super cell, both of the orthorhombic 25% Sr-doped $LaMnO_3$ structure. Surface and bulk are modeled independently of each other on the density functional theory (DFT) level (Sec. II A). The exchange of cations between bulk and surface is modeled in an *ab initio* thermodynamics approach (Sec. II B) where the bulk and surface models are considered to be in equilibrium with each other. The stable surface termination is determined by minimizing the grand potential (surface free energy) as a function of the cation chemical potentials (determined by bulk DFT calculations), the oxygen chemical potential (as a function of temperature and oxygen partial pressure) and the surface energy (determined by surface slab DFT calculations).

A. DFT calculations

The density functional theory (DFT) calculations were performed using the Vienna *ab initio* simulation package (VASP) [71,72] using the Perdew-Burke-Ernberhof (PBE) functional [73] with a Hubbard-U correction [74] of 4 eV on the Mn $3d$ orbital [24]. An initial magnetic moment of 3.5 on Mn was sufficient to reliably converge the calculations into the ferromagnetic, half-metallic state. For bulk and surface computations meshes of $(6 \times 6 \times 4)$ and $(6 \times 6 \times 1)$ k points were chosen for primitive orthorhombic cells. Together with an energy cutoff of 550 eV this approach ensures convergence of total energies and bulk vacancy formation energies within 4 meV/atom. To reliably study surface segregation we model the LSM25(001) surface in a symmetric slab with 15–19 layers, corresponding to 7.5–9.5 ABO_3 bilayers. Surface free energies (cf. Sec. II B) and segregation energies are converged with respect to the slab thickness within 0.9 meV/Å^2 and 7 meV, respectively.

A well-known problem in the modeling of oxides arises from the overbinding of oxygen in the gas phase versus the bulk oxide. This error can be corrected by applying Wang's scheme [75] of fitting the deviation between computed and experimental formation energies of binary oxides. The O_2 overbinding correction in our case amounts to +1.03 eV.

Based on diffraction studies of $LaMnO_3$ (LMO), doped lanthanum manganites have been proposed to assume a cubic structure above 750 K; however, $LaMnO_3$ retains its orthorhombic symmetry despite the transition to a metrically cubic lattice upon annealing ([76] and references therein). We therefore assume orthorhombic symmetry for our model system, 25% Sr-doped $LaMnO_3$ ($La_{0.75}Sr_{0.25}MnO_3$, or LSM25). All our bulk and surface calculations are performed in a symmetry-free configuration with orthorhombic (*Pnma*) atom positions as a starting guess. However, the structural relaxation due to doping with Sr and the presence of other point defects or proximity to the surface is quite significant, so that the relaxed structure may locally deviate from orthorhombic symmetry.

B. Calculation of the surface free energy

The data were analyzed using an *ab initio* thermodynamics approach, where the stability of surface configuration i is computed as the grand potential Ω_i, which is a function of $p(O_2)$ and T in a grand canonical ensemble, and yields the surface tension:

$$\Omega_i = \frac{1}{A}\Bigg[E_{\mathrm{slab},i} - n_{\mathrm{bulk},i}E_{\mathrm{LSM25,\ bulk}} - \sum_j (n_{i,j} - x_j n_{\mathrm{bulk},i})\mu_j(T, p(\mathrm{O_2}))\Bigg]. \quad (1)$$

$E_{\mathrm{slab},i}$ and $E_{\mathrm{LSM25,\ bulk}}$ represent the DFT-calculated energies of the surface slab in configuration i and $n_{i,j}$ and x_j the number of species j in configuration i and the fraction of species j in the bulk reference (0.75, 0.25, 1, and 3 for La, Sr, Mn, and O, respectively). $n_{\mathrm{bulk},i}$ gives the number of bulk unit cells ABO_3 used as a reference for configuration i and is calculated as

$$n_{\mathrm{bulk},i} = \mathrm{Min}(n_{\mathrm{Sr},i} + n_{\mathrm{La},i}, n_{\mathrm{Mn},i}). \quad (2)$$

Equilibration of the bulk with the gas phase reflecting the nonstoichiometry of LSM25 is not considered in the present model, i.e., these site fractions as well as the bulk reference are considered to be independent of T and $p(O_2)$.

The chemical potentials of species j are denoted by μ_j. The chemical potentials of O_2 as a function of temperature are obtained from the NIST database [83]. Because we model the exchange of oxygen between the solid and gas phase at elevated temperatures, we need to also take into consideration the vibrational entropy of O in the bulk to obtain more quantitatively reliable results. With the estimate of 22.5 J K^{-1} mol^{-1} per lattice O from Lee *et al.* [62] the error of not considering

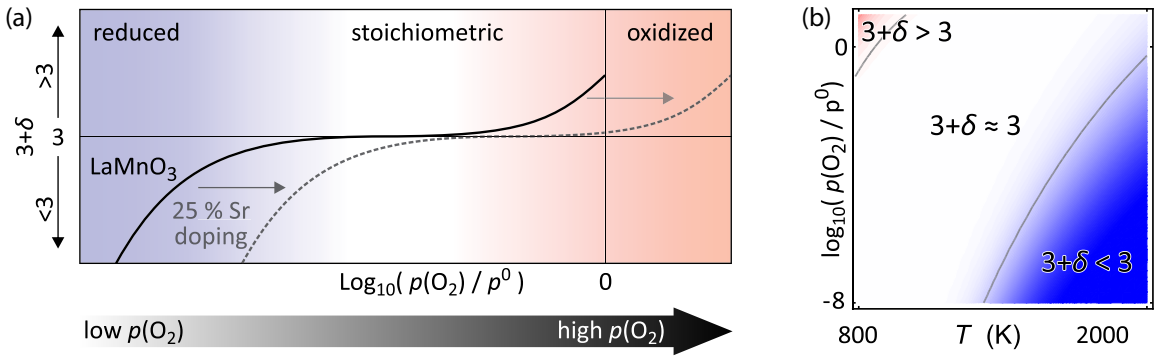

FIG. 1. Oxygen nonstoichiometry of (Sr-doped) $LaMnO_3$ (for details see Sec. S1 in Ref. [77] and Refs.[17,78–82]). (a) Scheme of oxygen content as function of $\log_{10}(p(O_2)/p^0)$ for pure $LaMnO_{3+\delta}$ and $La_{0.75}Sr_{0.25}MnO_{3+\delta}$. Three regimes can be identified: the reduced regime (blue), where $3+\delta < 3$, the stoichiometric regime (white), where $3+\delta \approx 3$, and and the oxidized regime (red), where $3+\delta > 3$. (b) Scheme of oxygen content as a function of T and $\log_{10}(p(O_2)/p^0)$, with oxygen content indicated by the color (red: oxidized, white: stoichiometric, and blue: reduced). Figure is adapted from Ref. [17].

the vibrational contribution of lattice oxygen would be 0.19 to 0.47 eV in the temperature range between 800 and 2000 K, which is quite significant and non-negligible. We note that the vibrational contribution of cation vibrations to the total energy is, in contrast, negligible. Although the total vibrational entropy is higher for the cations than for the oxide ions, the contribution to the segregation energy is canceled due to the low sensitivity of vibrational frequencies to the local chemical environment. According to our estimate, the error of neglecting this contribution is less than 0.05 eV, even at 2000 K because the entropy change between bulk and surface is rather small.

We model the exchange of cations between surface and bulk as a Schottky defect reaction, where cations from the bulk migrate to the surface to occupy empty lattice sites. The slabs and bulk super cells are overall charge-neutral, that is, the defect charges are balances by a local change of the Mn valence:

$$A^x_{A,\ \mathrm{bulk}} + 3\mathrm{Mn}^x_{B,\mathrm{bulk}} + \mathrm{V}^{'''}_{A,\ \mathrm{surf}} + 3\mathrm{Mn}^{\cdot}_{B,\mathrm{surf}} = \mathrm{V}^{'''}_{A,\ \mathrm{bulk}} + 3\mathrm{Mn}^{\cdot}_{B,\mathrm{bulk}} + \mathrm{A}^x_{A,\ \mathrm{surf}} + 3\mathrm{Mn}^x_{B,\mathrm{surf}}. \quad (3)$$

The energy cost of moving a cation from the bulk to the surface is therefore connected to the bulk vacancy formation energy. For the cations, Sr, La, and Mn, the chemical potentials were calculated from bulk DFT energies as

$$\mu_i = \left(\frac{dG_{\mathrm{bulk}}}{dn_i}\right)_{j\neq i} \approx \left(\frac{dE_{\mathrm{bulk}}}{dn_i}\right)_{j\neq i}, \quad (4)$$

neglecting entropy contributions. $(\frac{dE_{\mathrm{bulk}}}{dn_i})$ was estimated from the energy change of transferring a cation from the stoichiometric LSM25 bulk to the reference, that is, from the bulk into the gas phase. This value is calculated in a 64-unit supercell ($La_{48}Sr_{16}Mn_{64}O_{192}$). The concentration change is therefore 1.5%. The bulk acts as an infinite reservoir, which means that each cation removed from the bulk has the same energy, reflecting the removal of a cation from the stoichiometric bulk. Stoichiometric LSM25 is the best choice to model SOFC operation because LSM25 is near-stoichiometric over most of the relevant temperature and $p(O_2)$ range [indicated by the white area in Fig. 1(b)].

Favoring explicitly calculated numbers for the cation chemical potentials has both advantages and disadvantages compared to treating them as variable, using neighboring phases in the phase diagram as constraints, as previously done in the literature [61]. One the one hand, computing the chemical potentials explicitly allows us to establish a quantitative connection between the experimental conditions (T, $p(O_2)$) and the surface composition (termination, dopant and defect concentrations) for the first time. Rather than studying just a few defect-free terminations, we now have access to the rich defect chemistry of LSM25, which is exactly what we need in order to study dopant segregation. On the other hand, our approach is an approximation that is valid only under conditions where the LSM25 bulk composition is close to stoichiometric, which limits the applicability of our approach to a certain range of (T, $p(O_2)$), as discussed below. Because of these limitations, the present discussion will be restricted to stoichiometric $La_{0.75}Sr_{0.25}Mn_1O_3$ (LSM25), for which the chemical potentials of La, Sr, and Mn (referenced to isolated atoms in the gas phase) were determined as −12.78, −7.85, and −6.95 eV, respectively.

The choice of reference is generally arbitrary, and other choices (such as metals or oxides) are valid and have been employed in the literature (a quantitative comparison of different references for transferring and comparing our results with other studies in the literature is provided in Sec. S2 in Ref. [77]). Our chemical potentials determined for LSM25 are lower than those of metallic and oxidic references, showing that LSM25 is thermodynamically stable in this region. Our chemical potentials are quantitatively within the stability region of $La_{7/8}Sr_{1/8}MnO_3$ given by Piskunov *et al.* [61].

The approximation noted above is strictly valid only for the range in T and $p(O_2)$, where LSM is stoichiometric [area indicated in white in Fig. 1(b)]. In this range, the change in bulk (defect) concentrations due to exchange of cations and anions with the environment is negligible. Since the approximation also assumes that the bulk can be considered as an infinite reservoir of cations and vacancies, whose bulk concentrations are not affected by changes close to the surface, it is only

applicable to samples with low surface area. However, as shown by Piskunov *et al.*, cation chemical potentials in a nonstoichiometric compound can vary over several eV [61]. This means that our approximation is quite restrictive and gives rise to systematic errors due to the assumption that LSM25 is always stoichiometric. Quantitatively computing these chemical potentials as a function of T, $p(O_2)$ and x, y in $(La_{1-x}Sr_x)_yMnO_{3+\delta}$ is possible, but requires extensive calculations of the LSM bulk defect chemistry.

We also note that this approach of exchanging cations between bulk super cells and surface slabs requires well-converged computations in order to not introduce spurious energy contributions. The overall error of this approach was estimated by calculating the energy difference of exchanging La by Sr in a bulk super cell (which corresponds to $\mu_{La} - \mu_{Sr} = -4.93\,eV$) and in the center of a surface slab. The root mean square deviation determined for 11 different surface configurations is 0.14 eV or $4.6\,meV/Å^2$. This error magnitude is lower than the mean square deviation between two different random bulk configurations ($\approx$0.2 eV), which determines the error of our fitted chemical potentials. As a result, we conclude that our approach of calculating the surface free energy does not introduce significant errors.

III. RESULTS

A. Enrichment and depletion of defects at polar LSM25(001) surfaces

To examine the stabilities of LSM25(001) surface terminations and how they are affected by the segregation of point defects, we employed *ab initio* thermodynamics over a wide range of surface compositions and defect arrangements. We considered oxygen vacancies $V_O^{\cdot\cdot}$ and adsorbed oxygen O_{ad}, A-site cation vacancies $V_A^{'''}$ and La substitution by Sr ($Sr_{La}^{'}$), Mn interstitials $Mn_i^{\cdot\cdot\cdot\cdot}$, and Mn antisite defects Mn_{La}^{x}, as well as coexistence of these defects in the subsurface region (represented by a surface slab model) in associated and nonassociated configurations. To model different defect concentrations near the surface we employed different super cell sizes and shapes of surface slabs ((1 × 1), (1 × 2), (2 × 1), (2 × 2), $(\sqrt{2}\times\sqrt{2})R45°$), resulting in defect concentrations between $\frac{1}{8}$ and $\frac{1}{2}$ per surface unit cell. We also examined a variety of different AO and BO_2 surface terminations (MnO_2, LaO, SrO, mixed (La,Sr)O), as well as terminations with two and more subsequent AO layers (LaO-SrO and SrO-SrO).

Considering such a large configurational space results in a very large number of possible surface configurations (represented by termination and surface/subsurface point defects). Naturally, it is impossible to compute all possible configurations with DFT. To make this undertaking feasible, we exploit the fact that the pure electrostatic energy correlates well with the total energy calculated by DFT [24]. Using the pure electrostatic energy calculated by the Ewald sum as an estimate [84], we preselect configurations using a simulated annealing Monte Carlo approach (described in Sec. S3 in Ref. [77]). In total, over 450 different configurations were selected for the DFT data set.

For the purpose of relating the surface tensions with Sr enrichment at the surface, we define the near-surface Sr content

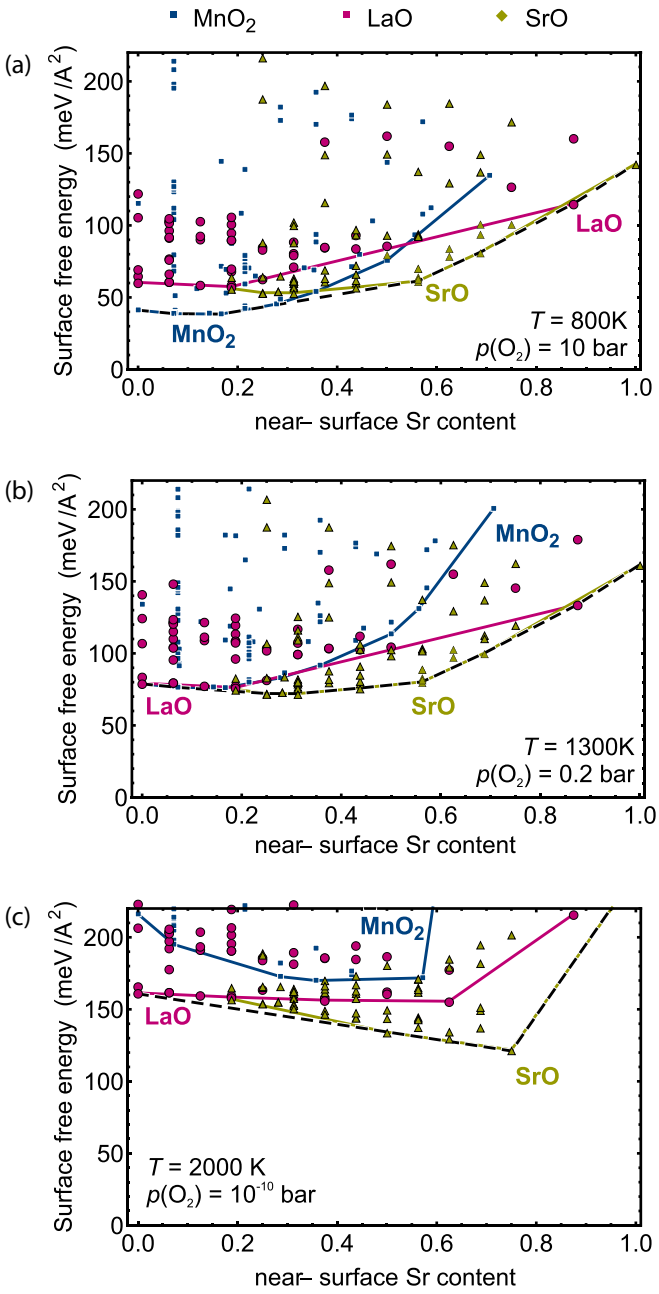

FIG. 2. Surface free energies of MnO_2, LaO, and SrO terminations at (a) 800 K, 10 bar O_2, (b) 1300 K and 0.2 bar O_2, and (c) 2000 K and 10^{-10} bar O_2 as a function of near-surface Sr content on $La_{0.75}Sr_{0.25}MnO_3(001)$ given by Eq. (5). The convex hulls for each termination are indicated by solid lines. The overall convex hull is shown by the black, dashed line. The results can be displayed for different (T, $p(O_2)$) conditions in Ref. [77].

for each calculated surface configuration $x(Sr)$ as

$$x(\mathrm{Sr}) = \frac{n_{\mathrm{Sr,slab}}}{n_{\mathrm{Sr,slab}} + n_{\mathrm{La,slab}}}, \tag{5}$$

where $n_{Sr,slab}$ and $n_{La,slab}$ stand for the number of Sr and La cations in the slab model that represents the near-surface region of LSM25. The surface tensions at 1300 K in air [$p(O_2) = 0.2$ bar] are plotted as a function of the near-surface Sr content in Fig. 2.

TABLE I. Surface enrichment and depletion of dominant ionic defects in oxidizing, stoichiometric and reducing regime as given in Fig. 1(b).

	oxidizing		stoichiometric		reducing	
bulk dominant ionic defect	$Sr_{La}^{'}$	$V_{La}^{'''}$, $V_{Mn}^{'''}$	$Sr_{La}^{'}$	other defect	$Sr_{La}^{'}$	$V_{O}^{\cdot\cdot}$
MnO_2	depleted	depleted	depleted	$V_{O}^{\cdot\cdot}$	enriched	enriched
LaO	depleted	enriched	depleted	$V_{La}^{'''}$	depleted	depleted
SrO	depleted	enriched	–	$V_{La}^{'''}$	enriched	enriched

The different terminations occupy well-defined areas in the diagram in Fig. 2 delimited by convex hulls indicated by lines connecting the lowest-energy structures for each termination under oxidizing [low T, high $p(O_2)$] and reducing conditions [high T, low $p(O_2)$]. The T and $p(O_2)$ values represented in Figs. 2(a)–2(c) are consistent with the oxygen stoichiometry regimes (oxidized, stoichiometric, reduced) indicated in Fig. 1(b). The free energies of the MnO_2, LaO, and SrO terminations are shown in blue, pink, and khaki, respectively.

The relative energies of convex hull minima allow us to infer the stabilities of the three terminations, as well as the near-surface Sr content. Under oxidizing conditions [Fig. 2(a)], the most stable termination is Sr-depleted MnO_2, followed by Sr-enriched SrO and Sr-depleted LaO. Under stoichiometric [Fig. 2(b)] and reducing conditions [Fig. 2(c)], the order reverses with Sr-enriched SrO having the lowest surface free energy, followed by Sr-depleted LaO and finally Sr-depleted MnO_2. The MnO_2 termination has a higher oxygen content than the LaO and SrO termination, thus being favorable at oxidizing conditions and unfavorable at reducing conditions. LaO and SrO have equal numbers of O, so that their energetic sequence does not change as a function of $\mu(O_2)$.

Beside the most favorable termination and its Sr content, the calculation also allows us to infer the respective dominant defect (listed in Table I for overview) at the surface as a function of $\mu(O_2)$ as will be shown in detail in the following sections.

1. MnO_2 *termination*

Under oxidizing conditions [Fig. 2(a)], the most favored MnO_2-terminated surface has a perfect, Sr-depleted configuration without oxygen or cation vacancies or adsorbed oxygen as shown in Fig. 3(a). This indicates that the previously proposed segregation of oxygen vacancies to the MnO_2 surface and subsequent segregation of Sr [24–26,51] does not contribute to the stabilization of the negative MnO_2 surface under these conditions. This is because oxygen vacancies raise the surface free energy rather than lowering it due to the high oxygen chemical potential in the gas phase. Under stoichiometric [Fig. 2(b)] and reducing [Fig. 2(c)] conditions, surface configurations with oxygen vacancies and high near-surface Sr concentrations constitute the lowest free energy configurations. This is indicated by the shift of the convex hull minimum from lower to higher near-surface Sr content. This reinforces the previous discussions about the interplay between surface reduction and Sr segregation at the MnO_2 terminations. However, under these conditions the MnO_2 termination is not dominant since the SrO termination is significantly lower in surface free energy, making the relevance of this finding in explaining Sr segregation questionable.

2. LaO *termination*

The most stable LaO-terminated surfaces with their positive surface dipole moment are more diverse, either featuring adsorbed O or surface-segregated A-site cation vacancies without or with very little near-surface Sr, all of which are negatively charged defects. Under oxidizing, stoichiometric and reducing conditions [Figs. 2(a)–2(c)], the LaO termination supports a high A-site cation vacancy concentration with up to $\frac{1}{4}$ La cations missing in the termination layer. Configurations with adsorbed oxygen are only $10-20\,\mathrm{meV/Å^2}$ higher in surface free energy at 800 K and 10 bar O_2, indicating that areas of the LaO termination without cation vacancies are most likely covered by adsorbed oxygen under these conditions. As the gas phase conditions go from oxidizing to reducing, both positively charged oxygen vacancies and negatively charged Sr are enriched at the surface. As a consequence, the minimum of the convex hull for the LaO termination shifts from 0.2 (Sr-depleted) to 0.6 (Sr-enriched). This result supports previous hypotheses that enrichment of Sr near the surface is a consequence of the electrostatic attraction between oxygen vacancies and the Sr dopant [24–26,51].

The stability of the LaO termination is greatly enhanced by the presence of cation vacancies due to the opposite charges of $V_{cation}^{'''}$ and the positively charged LaO termination. For instance, at 1300 K and 0.2 bar O_2, all the points on the convex hull have A-site vacancies at the surface, and the free energies of these terminations are at $80\,\mathrm{meV/Å^2}$ (same as the free energies of the MnO_2 termination). In contrast, the surface free energy of a defect-free LaO termination is at around $190\,\mathrm{meV/Å^2}$ under these conditions, and the temperature where the MnO_2 termination becomes less favorable than the LaO termination is at over 2000 K, similar to the predictions by Piskunov *et al.* [61]. This highlights how strongly near-surface point defects can influence the relative stabilities of different terminations at the surface.

3. SrO *termination*

Like the LaO termination, the SrO termination has a slightly positive dipole moment, thus attracting negatively charged point defects such as cation vacancies and Sr. The SrO termination on LSM25(001) behaves like the SrO termination on $SrTiO_3$ in this regard, as noted in the introduction and further elucidated in a Bader charge analysis (see Sec. S4 in Ref. [77] for details). However, due to the weaker dipole moment of the SrO termination compared to the LaO termination (cf. Sec. III C), positively charged point defects

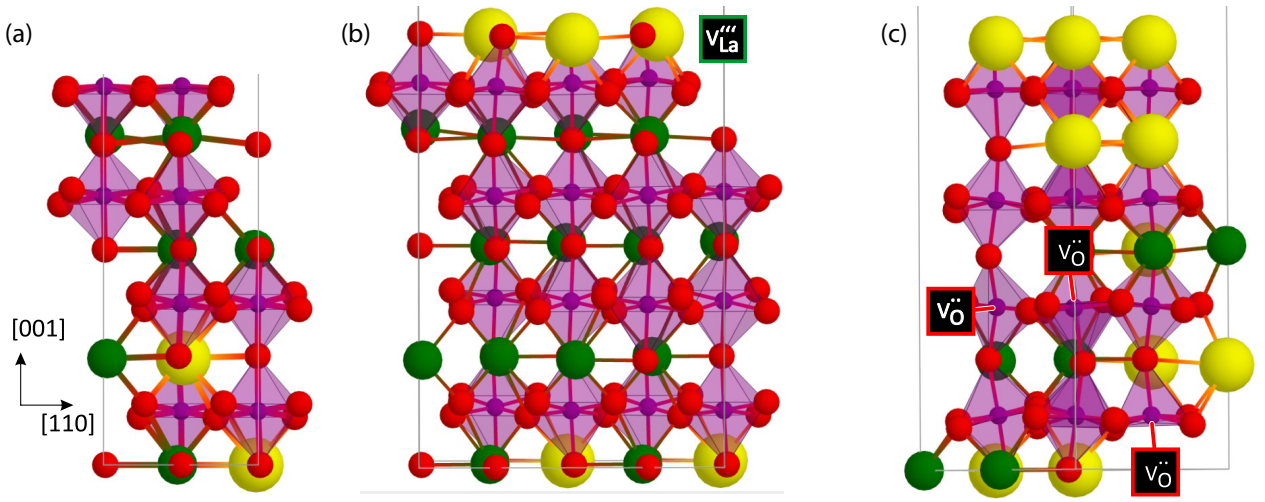

FIG. 3. Most favorable configurations for the fully covering terminations [minima of convex hulls in Figs. 2(a)–2(c)] with defects indicated by black boxes. (a) Vacancy-free, Sr-depleted MnO_2 termination stable under oxidizing conditions, (b) SrO termination with *A*-site (Sr/La) vacancy in the termination layer under stoichiometric conditions, and (c) Sr-oxide terminated surface highly enriched in oxygen vacancies and Sr under reducing conditions. Colors represent: green - La, yellow - Sr, purple - Mn, and red - O.

such as oxygen vacancies can also be stable. Under oxidizing and stoichiometric conditions [Figs. 2(a) and 2(b)], the most favorable surface configuration features *A*-site cation vacancies (1/4) at the surface and subsurface Sr in addition to the SrO termination layer as shown in Fig. 3(b). However, the overall near-surface Sr content as given by the minimum of the convex hull is equal to the bulk nominal value (0.25) under oxidizing conditions. Configurations with higher subsurface Sr contents are close in surface free energy (> 5 meV) and may coexist with *A*-site vacancies. Under reducing conditions [Fig. 2(c)] the most stable surface configurations feature a concentration of oxygen vacancies around 2%–3%. The increased positive surface charge leads to enrichment of Sr near the surface as indicated by the shift of the convex hull minimum from 0.25 at stoichiometric to 0.8 at reducing conditions. The configuration is shown in Fig. 3(c). This is again in line with the previously mentioned hypothesis of surface reduction leading to an enrichment of Sr near the surface. Our results show that this hypothesis is at least qualitatively equally applicable to the SrO termination as to the MnO_2 termination for which it was originally proposed. Larger near-surface Sr contents were not studied for the SrO termination although the minimum of the convex hull has apparently not yet been reached in Fig. 2(c). This is because the structure approaches $SrMnO_3$ already for 80% near-surface Sr content. $SrMnO_3$, however, is not stable in the orthorhombic perovskite structure [85,86]. We will show in the next section that a different surface termination with a lower near-surface Sr content is substantially more stable under reducing conditions.

B. Nonpolar LSM25(001) surface reconstructions

The previous section considers only terminations whose termination layer is fully covering at the surface, i.e., only one termination (*AO* or BO_2) is exposed to the surface. We have seen in Sec. III A that without near-surface defects neither of these MnO_2, LaO, and SrO terminations has zero dipole moment. However, one can imagine coexistence of two terminations at the surface, resulting in areas with positive and negative dipole moments, and such opposite dipoles canceling each other. This may result in patterning of the surface or growth of steps on the atomic scale.

This can be modeled by pairing anion and cation vacancies at the surface, revealing the underlying layer. To distinguish these terminations from the fully covering termination with only single defects, we refer to these configurations with associated vacancies in the termination layer as "partial" LaO/SrO/MnO_2 terminations. Our database contains 185 configurations of this type. These cation and anion vacancies attract each other due to opposing charges, typically resulting in an association energy of -0.8 to -1 eV in the bulk and behaving similar to a single vacancy with a lower charge in terms of energy. Similar vacancy association energies were obtained for test cases at the surface, resulting in a substantial stabilization of such defect associates. Accumulation of vacancy associates at the surface leads to the exposure of significant portions of cations and anions in the underlying layer. For example, a $[V_{A/B}^{'''} - V_O^{\cdot\cdot}]$ exposes not only the underlying oxygen, but also the *B* cations in the case of the *AO* termination, and A cations in the case of the BO_2 termination. The presence of vacancy cluster has potential consequences for the interaction of the surface with the surrounding gas atmosphere. Exposing portions of both BO_2 and *AO* terminations to the gas phase and the possibility to adjust the cation to anion ratio in the termination layer enables additional degrees of freedom for the surface to reduce its dipole moment and surface free energy.

The surface free energies of the partial terminations are plotted as red, yellow, and teal dots and curves in Fig. 4 for the partial LaO, SrO, and MnO_2 terminations, respectively. The convex hulls of the previously discussed LaO, SrO, and MnO_2 perfect terminations (Fig. 2) are plotted as reference in the figures. As can be inferred from the convex hulls, the partial terminations can be more stable than the entirely

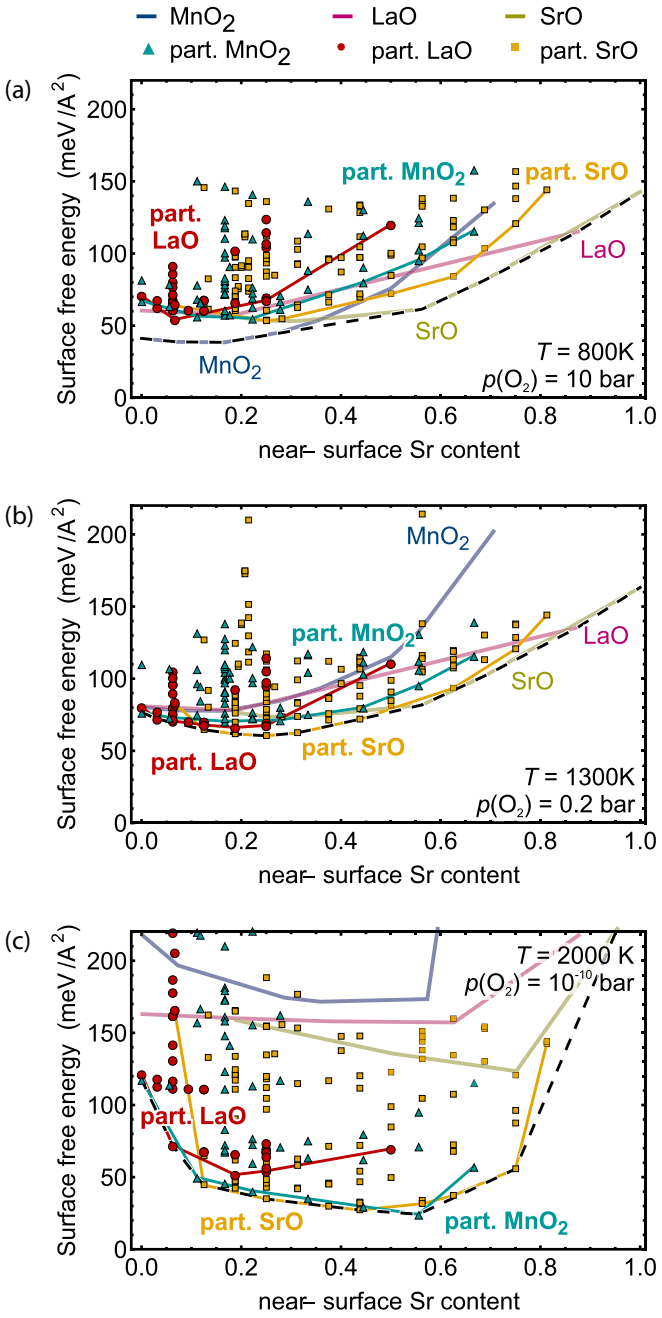

FIG. 4. Free energies of partially covering terminations plotted together with the convex hulls for the fully covering terminations from Fig. 2 at (a) 800 K and 10 bar O_2, (b) 1300 K and 1 bar O_2, and (c) 2000 K and 10^{-10} bar O_2. For ease of comparison, only the convex hull lines (and not the data points) of the fully covering terminations from Fig. 2 are shown. The free energy is plotted as a function of near-surface Sr content at the surface of the $La_{0.75}Sr_{0.25}MnO_3(001)$. The convex hulls for each termination are indicated by solid lines. The overall convex hull that minimizes the free energy for all considered configurations is shown by a black, dashed line. The results can be displayed at different $(T, p(O_2))$ conditions in Ref. [77].

covering terminations and the Sr content where the surface free energy is minimized differs between partial and perfect terminations.

Figure 4 shows the free energy curves as a function of the near-surface Sr content for the partial terminations together with the fully covering terminations. The partial MnO_2, LaO and SrO terminations are drawn in teal, red, and yellow, respectively

Under oxidizing conditions, the stabilities of all three partial terminations fall into the same free energy range as the fully covering LaO and SrO terminations [Fig. 4(a)]. The fully covering MnO_2 termination still has the lowest surface free energy [blue convex hull in Fig. 4(a)] so that our previous conclusion about the most stable termination does not change by considering these new structures. Under stoichiometric conditions [Fig. 4(b)], all three partial terminations are slightly more stable than the SrO termination. The most stable termination is now the partial SrO termination [shown in Fig. 5(a)] with the surface free energy minimized at a near-surface Sr content of 0.25, which conforms with the nominal bulk Sr content. Both enrichment and depletion of Sr, as well as the introduction of additional cation or oxygen vacancies lead to an increase of the surface free energy under these conditions.

Under reducing conditions [Fig. 4(c)], the partial terminations are lower in energy by over 100 meV/Å^2 compared to the fully covering terminations. The partial SrO and MnO_2 terminations show similar overall stability and trend with near-surface Sr content [cf. teal and yellow convex hulls in Fig. 4(c)]. The partial MnO_2 termination minimizes the surface free energy at a near-surface Sr content of 0.55. This configuration [shown in Fig. 5(c)] consists of an $[Mn_2O_2]^{2+}$ chain adsorbed on a mixed (Sr, La)O layer. The positively charged $[Mn_2O_2]^{2+}$ chain attracts large amounts of Sr'_{La} to the surface as clearly depicted in Fig. 5(c). A similar surface stability [cf. teal and yellow convex hulls in Fig. 4(c)] is achieved by surface configurations that consist of adsorbed Sr^{2+} cations adsorbed on top on an MnO_2 layer [Fig. 5(b)]. Similar to Fig. 5(c), the positive charge on the surface attracts Sr cations close to the surface. For this termination, different Sr contents and arrangements in the slab were considered, and the surface free energy was minimized for the configuration with the topmost layer of La^{3+} cations replaced by Sr^{2+} as shown in Fig. 5(b).

At this point we cannot say for certain that either Fig. 5(b) or 5(c) constitutes the most stable surface termination due to the approximations we make and the sheer number of possible surface configurations: In the computation of the surface free energy we assume that the chemical potentials of cations in the bulk reference are constant, as determined for stoichiometric LSM25 (cf. Sec. II B). Under highly oxidizing and highly reducing conditions [cf. Fig. 1(b)], the LSM25 bulk is oxidized and reduced, respectively, leading to significant deviations of the chemical potentials from the stoichiometric values. From our error analysis we conclude that the SrO coverage on the surface is possibly underestimated under reducing conditions due to the increase of the Sr chemical potential under reducing conditions (see Sec. S5 in Ref. [77] for an estimate of μ_{Sr} as a function of T and $p(O_2)$).

Finally, we note that the surface free energy under reducing conditions [Fig. 4(c)] approaches zero. A computed surface free energy at or below zero indicates decomposition of the bulk material. LSM25 is well-known to decompose under highly reducing conditions [82,87,88] at an oxygen content

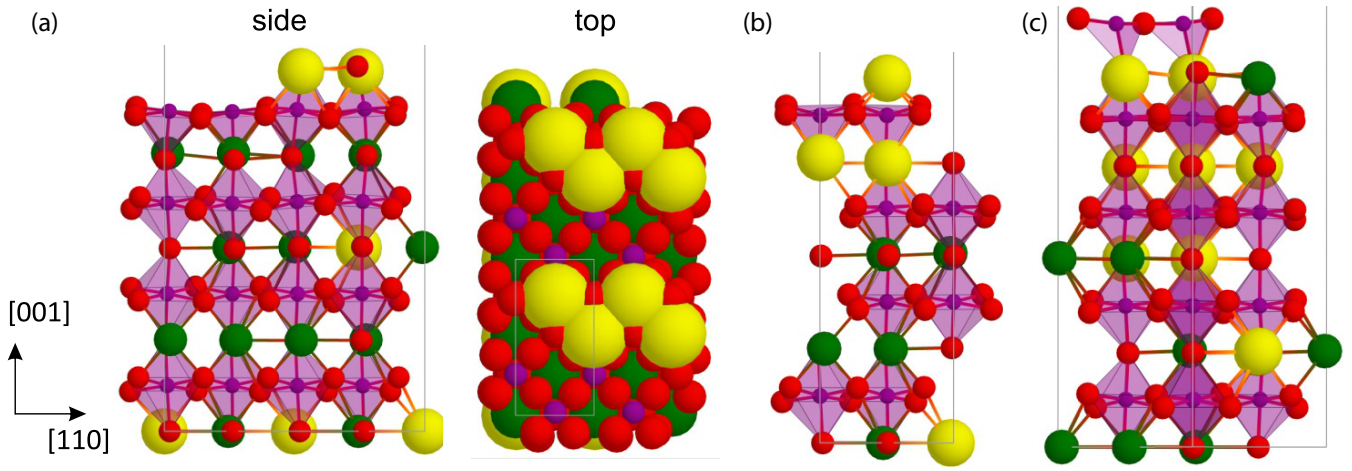

FIG. 5. Favorable partially covering terminations. (a) Stoichiometric conditions: partial SrO termination with a [SrO] coverage of ½, side and top view. [(b) and (c)] Two of the most stable configurations under reducing conditions. (b) Sr cation adsorbed on MnO_2 termination, Sr enriched. (c) $[Mn_2O_2]$ cluster adsorbed on the Sr-enriched surface. Colors represent: green - La, yellow - Sr, purple - Mn, and red - O.

below 2.85 [88]. Our model is able to reproduce this fundamental property of LSM25, and even the oxygen content where decomposition occurs is in the same range (2.88). While this appears as a minor detail, we conclude from this observation that our model can describe LSM25 reliably even in the highly reducing range of temperature and $p(O_2)$.

We emphasize that these results show a very clear trend, despite the quantitative uncertainties; that is, oxygen deficient and thereby positively charged surface layers, such as $[MnO_x]^{(3-2x)+}$ clusters or adsorbed Sr^{2+} cations constitute stable surface configurations. This excess positive charge at the surface is compensated by Sr enrichment within the perovskite lattice close to the surface. This is particularly striking in the case of Fig. 5(c), where almost all La^{3+} in the three topmost layers are replaced by Sr^{2+}. This trend is in line with our findings for all the fully covering terminations (Sec. III A), where configurations with coexisting $V_O^{\cdot\cdot}$ and Sr'_{La} minimize the surface free energy under reducing conditions. We thereby conclude that the trend of more Sr enrichment with more reducing conditions holds, regardless of whether we consider only fully covering terminations, or include partial terminations in the model as well.

Using all the information about the stable terminations, we can now plot a surface phase diagram that shows the stable surface configuration, which includes termination and dominant defect, as a function of T and $p(O_2)$ as shown in Fig. 6. Going from oxidizing (top left) to reducing (bottom right) conditions, we identify four different stable surface termination. Under oxidizing conditions [blue area (a)], the surface is MnO_2-terminated without point defects near the surface. The structure is shown in Fig. 3(a). In the area where LSM25 has a stoichiometric composition [green area (b)], the partial SrO termination with 50% SrO coverage and a total near-surface Sr content near 0.25 dominates [cf. Fig. 5(a)]. Going to even more reducing conditions, there is a slim purple band that represents a configuration similar to the previous one (partial SrO termination shown in [cf. Fig. 5(a)] that has one additional oxygen vacancy in the termination layer, resulting in a Sr/O ratio of the termination of 2/1. The additional oxygen vacancy leads to enrichment of Sr near the surface to 0.45. Under very reducing conditions the termination switches to a strongly reduced partial MnO_2 termination with 50% and 25% occupation of Mn and O, respectively, shown in cf. Fig. 5(c). The Mn/O ratio in this surface termination is 1/1 as opposed to ½ in a termination devoid of oxygen vacancies. This surface is strongly reduced, which also leads to significant near-surface Sr enrichment of 55% as given by the minimum of the convex hull in Fig. 4(c).

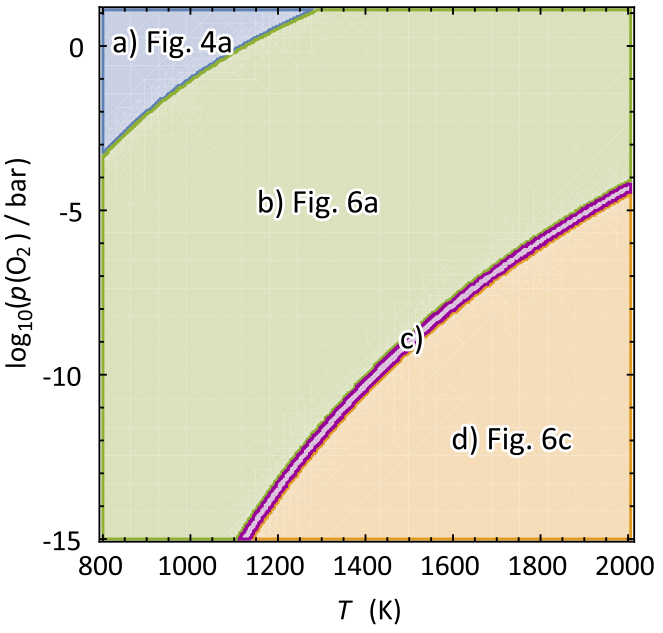

FIG. 6. Surface phase diagram of the $La_{0.75}Sr_{0.25}MnO_3(001)$ surface as a function of T and $p(O_2)$. The configurations that appear in this diagram are (a) blue/oxidizing: Sr-depleted MnO_2 termination [Fig. 3(a)], (b) green/stoichiometric: partial SrO termination [Fig. 5(a)], (c) red/stoichiometric-to-oxidizing, same as (b), with an additional $V_O^{\cdot\cdot}$ in the termination layer and Sr enriched near the surface, and (d) orange/reducing: Sr-enriched partial MnO_2 termination with additional $V_O^{\cdot\cdot}$ [Fig. 5(c)].

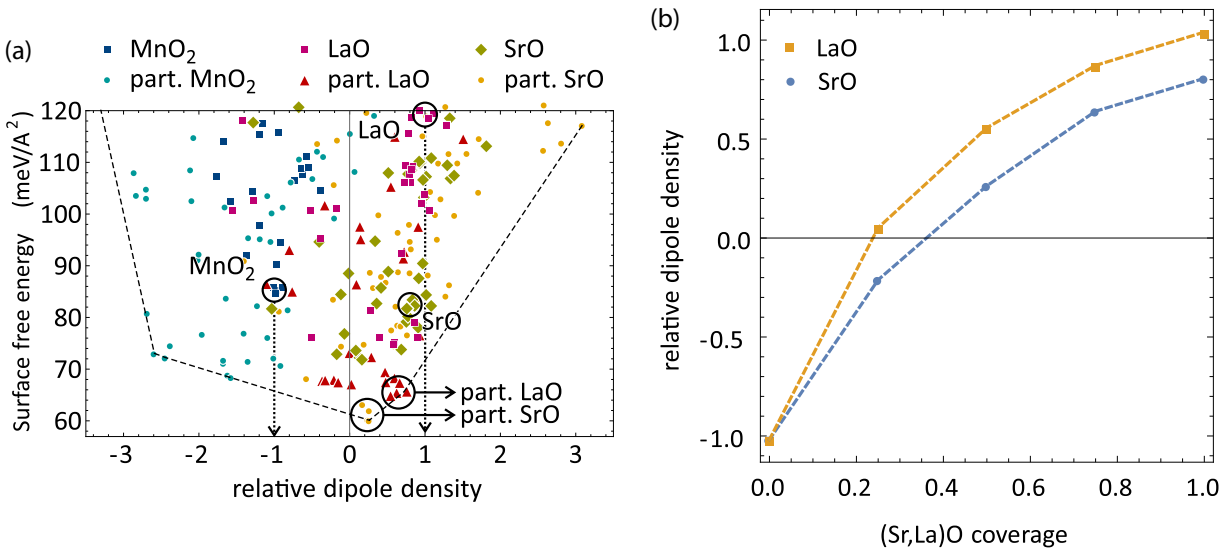

FIG. 7. (a) Surface free energy as a function of the relative surface dipole density, color-coded by termination at 1300 K, 0.2 bar O_2 (stoichiometric conditions). The clean, defect-free MnO_2 and LaO terminations were chosen as negative (-1) and positive ($+1$) references for the relative dipole density, as indicated in the diagram. The convex hull is indicated by the black, dashed line. The results can be displayed for different (T, $p(O_2)$) conditions in Ref. [77]. (b) Relative dipole density for partial SrO and LaO terminations, as a function of coverage, with 0 and 1 representing the MnO_2 surface and the fully covering SrO and LaO terminations, respectively.

C. Why the partial SrO termination is so stable

The MnO_2 and LaO terminations are pure Tasker type 3 surfaces [47], where the alternating +1/-1 stacking of charges is truncated at the surface, giving the surface a permanent dipole moment. The SrO termination is not a pure Tasker type 3 surface because the termination layer has a significantly lower charge than the layers below and, in that, is similar to a Tasker type 2 surface. In order to obtain more quantitative information on the polarities of surfaces with and without charged point defects, we computed the work function for each of our surface slabs from the difference between the total potential in the slab center and the fermi energy. The work function is assumed to be proportional to the dipole density of the surface [89]. To correlate the work function with the relative dipole density, we set the dipole densities of the clean, defect-free MnO_2 and LaO terminations to -1 and $+1$ as references. The dipole densities of all the computed configurations are shown in Fig. 7(a), where the MnO_2 and LaO references, as well as the perfect SrO termination are marked by circles. The relative dipole density of the SrO termination is close to the value of the LaO termination, i.e., positive. From this, we conclude that, while the SrO termination has a lower dipole moment, it does not constitute a neutral termination.

In Sec. III B, we proposed a partial SrO termination, which consists of [SrO] stripes on top of the MnO_2 termination, which is also indicated in Fig. 7(a) ("part. SrO"). The relative dipole density for this surface termination is close to zero, indicating a nearly charge-neutral surface. The partial LaO termination is slightly more positive, as indicated in Fig. 7(a) ("part. LaO"). These points indicate partial terminations where half the surface is covered by (La,Sr)O, but the coverage is in principle variable. The numerically determined relative dipole densities of partial SrO and LaO terminations without additional point defects are plotted as a function of the AO coverage in Fig. 7(b). For both partial terminations, the surface becomes increasingly positive with increasing AO coverage. The positive surface charge increases more steeply with coverage for the LaO termination due to the higher positive charge per LaO pair ($+1.99 - 1.33 = +0.66$) compared to a SrO pair ($+1.57 - 1.22 = +0.37$). For the partial SrO and LaO terminations, the coverages that minimize the relative dipole magnitude densities are between 0.25 and 0.5 (SrO), and close to 0.25 (LaO).

The surface dipole density is strongly correlated with the surface stability, which can be visualized by plotting the surface free energy versus the dipole density [Fig. 7(a)]. This confirms that the surface free energy at 1300 K and 0.2 bar O_2 is minimized at a surface dipole density close to zero, while the strongly polar MnO_2 and LaO terminations have significantly higher surface free energies. However, this does not imply that the surface must be charge-neutral under all conditions. Rather, it can be shown by computing the average surface dipole density as a function of (T, $p(O_2)$) (see Sec. S 6 in Ref. [77] for more detailed information on the interplay of surface polarity and near-surface Sr enrichment) that the surface is on average more negative under oxidizing and more positive under reducing conditions. The more positive surface charge is a result of the increased formation of oxygen vacancies ($V_O^{\cdot\cdot}$) under reducing conditions that has deep implications for the enrichment and depletion of Sr near the surface, as will be shown in the next section.

D. The surface is stabilized by Sr enrichment under reducing conditions

We have seen in Sec. III B that the minimum of the convex hull shifts to higher Sr concentration within the near-surface

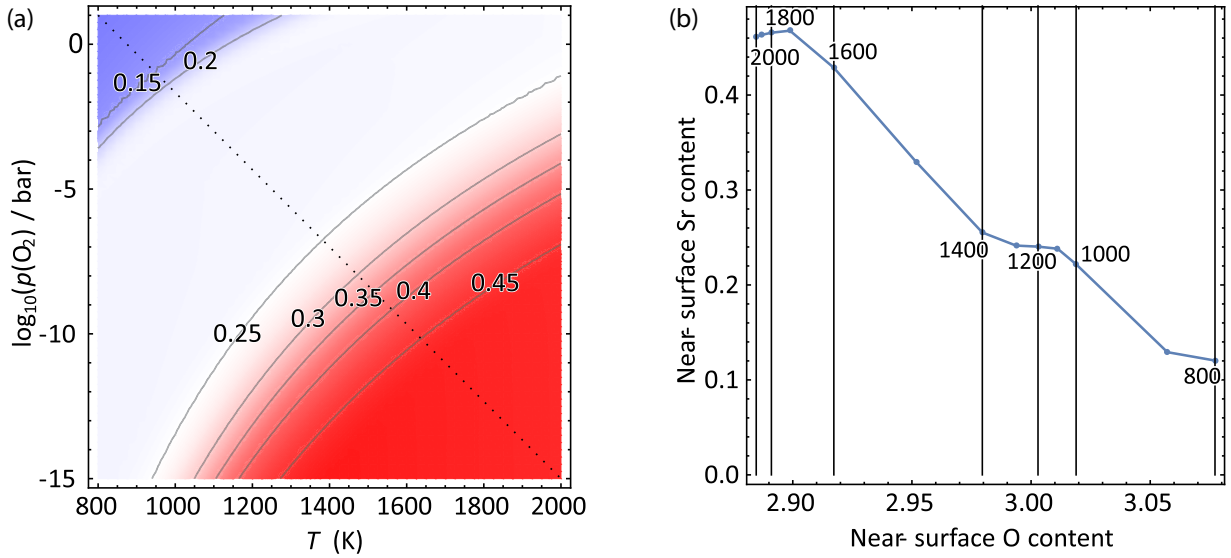

FIG. 8. (a) Near-surface Sr content [Eq. (5)] for LSM25, averaged over the convex hull [using Eq. (7)] as a function of T and $\log_{10}(p(O_2)/\text{bar})$. Individual diagrams of the surface free energy as a function of $x(O)$ as well as the averaged near-surface oxygen content can be displayed using Ref. [77]. (b) Correlation between near-surface oxygen content and near-surface Sr content, going along the dashed line in (a). Temperatures in degrees Kelvin are indicated in steps of 200 K.

region as conditions become more reducing. This finding was rationalized by considering the surface dipole density in Sec. III C. These findings leave two major questions unanswered: can we use these results to establish a firm connection between operating conditions and Sr surface enrichment? That is, can we predict the near-surface Sr content as a function of $(T, p(O_2))$? And can we correlate the Sr surface enrichment with surface reduction, that is, the near-surface oxygen content?

To answer these questions, we consider again the convex hulls computed as a function of the near-surface Sr content defined as

$$x(\text{Sr}) = \frac{n_{\text{Sr,slab}}}{n_{\text{Sr,slab}} + n_{\text{La,slab}}}, \tag{5}$$

where $n_{\text{Sr,slab}}$ and $n_{\text{La,slab}}$ denote the number of Sr and La atoms in the slab, regardless of their position within the slab. Similarly, we define the near-surface oxygen content as

$$x(\text{O}) = \frac{2n_{\text{O,slab}}}{n_{\text{Sr,slab}} + n_{\text{La,slab}} + n_{\text{Mn,slab}}}, \tag{6}$$

where $n_{\text{O,slab}}$ and $n_{\text{Mn,slab}}$ represent the number of oxygen and Mn atoms in the slab, respectively. We can now compute both the averaged near-surface Sr and oxygen contents as a function of $(T, p(O_2))$ using Eqs. (5) and (6). The averaged near-surface Sr content is computed as the integral over the convex hull:

$$\bar{X}(T, p(\text{O}_2)) \approx \frac{1}{Q(T, p(\text{O}_2))} \int_V x \times \exp\left[-\frac{E(x,\ T, p(\text{O}_2))}{k_B T}\right] dx \text{ with} \tag{7}$$

$$Q(T, p(\text{O}_2)) = \int_V \exp\left[-\frac{E(x, T, p(\text{O}_2))}{k_B T}\right] dx, \tag{8}$$

where x and $\bar{X}$ indicate the property and mean value of this property, $E(x, T, p(O_2))$ the surface free energy of the convex hull as a function of that property, temperature and $p(O_2)$, and V the range of possible values.

The averaged near-surface Sr content is given in Fig. 8(a), where the red-white-blue diagram displays the near-surface Sr content [Eq. (5)] color coded with white set to the nominal bulk Sr content (0.25). The blue and red regions thus represent Sr depletion [$x(\text{Sr}) < 0.25$] and Sr enrichment [$x(\text{Sr}) > 0.25$], respectively. In the top-left corner (oxidizing conditions) the surface will be Sr-depleted, which is reconciled with the results in Fig. 4(a), which show that the most the most favorable surface termination is a Sr-depleted MnO_2 termination. The surface remains somewhat Sr-depleted [$0.2 < x(\text{Sr}) < 0.25$] until well into the reducing regime (10^{-8} bar at 1300 K) indicated by the light-blue area, after which the near-surface Sr content steeply increases to values over 0.45. This steep increase under reducing conditions is hypothesized to be due to the favorable electrostatic interaction between V'_{Sr} and $V^{\cdot\cdot}_{O}$ as shown in the following.

The direct correlation between near-surface Sr enrichment and surface reduction is visualized in Fig. 8(b), answering the second question posed above. This figure plots the near-surface Sr content [$x(\text{Sr})$] versus the near-surface oxygen content [$x(\text{O})$] calculated along the black, dashed line in Fig. 8(a). Because the relationship between oxygen content and temperature is nonlinear, temperatures are also indicated in the diagram for reference. There is a clear correlation between Sr and O content near the surface, with increasing oxygen content leading to a decrease in Sr content. Near-surface Sr enrichment (over the bulk content of 0.25) takes place only under reducing conditions, at a near-surface oxygen content below 2.98 (or temperatures higher than 1400 K. The slight decrease of near-surface Sr content under very reducing conditions [$x(\text{O}) < 2.90$ and $T > 1800$ K is an artifact due to insufficient sampling of configurational space in this region.

IV. DISCUSSION

We employed density functional theory (DFT) calculations to study the surface and near-surface composition of 25% Sr-doped $LaMnO_3$ over a large range of T and $p(O_2)$, considering a variety of defects at and near the surface (Sr'_{La}, $V^{\cdot\cdot}_{O}$, $V^{'''}_{Mn}$, $V^{'''}_{La}$, O_{ad}) and different surface terminations [MnO_2, (Sr,La)O, partial MnO_2 and (Sr,La)O terminations, and SrO multilayers]. Because we consider simultaneously different terminations, different defects and coexistence of defects at the surface, we are able to quantify for the first time how surface defects influence the stabilities of surface terminations in LSM25. Combining the surface energies from over 450 surface configurations into a single *ab initio* thermodynamics model allows us to make quantitative predictions about the enrichment Sr on and near the surface as a function of temperature and $p(O_2)$. In addition, we propose a new surface termination for LSM25, which consists of [SrO] stripes on top the MnO_2 termination, which minimizes both the surface dipole moment and free energy in the (T, $p(O_2)$) range where LSM25 has stoichiometric composition.

The stabilization of point defects at different terminations of LSM at various Sr doping levels has been studied by a several groups in the past [24,42,60], and the general conclusion from these studies is that the polar terminations of LSM stabilize the defects with opposing charge. Our results confirm these findings from previous computational studies entirely and quantitatively (in the sense that we obtain the same defect formation and segregation energies reported in these studies). However, since the stability of charged defects is influenced by surface charge, the opposite is also true, i.e., the stabilities of charged surface terminations are changed by the presence of charged defects. Therefore we propose that conclusions about the relative stabilities of terminations at charged surfaces cannot be drawn without explicitly considering charged defects near the surface. We assess this hypothesis in the form of an *ab initio* thermodynamics model that considers explicitly the interaction of charged defects with the surface termination in evaluating the surface stability.

A. Stabilization of surface terminations and near-surface point defects

Our model provides a significant advancement compared to previous *ab initio* thermodynamics studies [61] that considered different terminations, but not how they are stabilized by near-surface points defects. While our results confirm the trends for the defect-free MnO_2, LaO, and SrO termination found in this previous investigation, we find that a defect-free termination (the MnO_2 termination) is stable only under slightly oxidizing conditions. Under all other conditions (strongly oxidizing, stoichiometric, reducing), the surface structures that minimize the surface free energies incorporate a high concentration of point defects in the percent range, such as cation vacancies under oxidizing, oxygen vacancies under reducing, and/or varying amounts of Sr'_{La} that balance the respective polarity of the surface. Moreover, incorporating defects into the surface model can alter the relative stabilities of the terminations as well as transition (T, $p(O_2)$), so that restricting thermodynamic considerations to defect-free surfaces can lead to misleading conclusions regarding the stable surface termination. We emphasize again that LSM is a highly nonstoichiometric material (as reflected by its full composition formula $(La_{1-x}Sr_x)_yMnO_{3+\delta}$) that can support oxygen or cation vacancy concentrations in the percent range. In this concentration range, these defects can significantly influence (both positively and negatively) the stabilities of surfaces and interfaces.

In addition, we explicitly consider associated defects, such as $[V^{\cdot\cdot}_{O} - V^{'''}_{La}]$ and $[V^{\cdot\cdot}_{O} - V^{'''}_{Mn}]$ in the surface termination layer, which gives rise to partially covering, or coexisting, terminations. The defect association energies are around 0.8 to 1.0 eV, thus, providing significant mutual stabilization of these vacancies that needs to be taken into consideration in the evaluation of surface free energies. These defect associates expose both metal and oxygen species of the underlying layer, thus allowing both types of A/B cations to interact with the gas phase. The partial coverage of a termination on the surface adds another degree of freedom in optimizing the surface structure and has not been considered in previous computational studies of LSM. One special property of these partial terminations is in gradual adjustment of the surface dipole moment. While the MnO_2 and (La,Sr)O terminations have negative and positive surface dipole moments, respectively, a surface partially covered with one of these terminations can be unpolar, which drastically alters the stabilities of defects in the near-surface region.

B. Sr surface enrichment under strongly reducing conditions

The relative surface stabilities as a function of (T, $p(O_2)$) are further employed to quantitatively compute near-surface enrichment of Sr, as well as the replacement of cations in the surface termination by Sr. This allows us to make quantitative predictions about the composition of the surface and near-surface region, as well as Sr segregation onset temperature and $p(O_2)$ for the first time. We emphasize, however, that these predictions are estimates at this point because we do not consider the equilibration of the LSM25 bulk reference with the gas phase. This approximation is strictly valid only within the stoichiometric region of LSM25 [cf. Fig. 1(b)]. Since Sr segregation mostly falls outside this region, the near-surface Sr content, as well as the SrO coverage on the surface under reducing conditions are underestimated by our current model, according to our error analysis (cf. Sec. S5). Extensive computations of the LSM25 bulk defect chemistry are required to correct this shortcoming, which will be undertaken in the near future.

Finally, we would like to note that *ab initio* thermodynamics models as presented in this contribution assume that the bulk of the material represents an infinite reservoir of ions and vacancies, and equilibration with the surface does not alter the bulk chemical potentials. This is true only for low-surface-area materials, such as single crystals, pellets or microporous specimens, but not for nanomaterials and, most importantly in the context of model studies, not for thin films. Consider for instance that a thin film with 20 nm thickness consists of only 50 ABO_3 layers. At 25% Sr substitution, only 12–13 Sr ions are available per column on average. The formation of a SrO termination or enrichment within the perovskite lattice

changes the Sr content as well as the A/B ratio in the bulk by roughly 2% per Sr cation migrated to the surface. This sounds like a small change, but it can reduce the bulk chemical potential of Sr by several eV, which is non-negligible. We emphasize that an *ab initio* thermodynamics model as presented here is not capable of quantitatively predicting the surface composition of thin films or other high-surface-area electrode materials. Doing so requires a self-consistent approach that explicitly takes into consideration the number of available ions and vacancies in the bulk in finite, for instance, by means of a Monte Carlo model. However, the qualitative trends predicted by our model can be transferred to thin films and other high-surface-area materials, even if the actual surface composition and reconstructions may deviate.

C. Comparison of the partial SrO termination with the $KTaO_3(001)$ labyrinth reconstruction

A similar termination has been discovered by Setvin *et al.* in a combined AFM and computational study on the $KTaO_3(001)$ surface [67]. This perovskite surface exhibits a similar (but reversed) stacking of charged KO (-1) and $TaO_2(+1)$ layers as LSM. This makes the pure terminations of the $KTaO_3(001)$ facet dipolar and highly unstable. After cleavage, the $KTaO_3(001)$ surface exposes a TaO_2 termination with disordered islands of KO on top of that. Upon annealing to 517 K, the structure reorders into a labyrinth reconstruction, which consists of alternating KO and TaO_2 stripes aligned in (110) and $(1\bar{1}0)$ directions. The experimental work is supported by density functional theory calculations that provide further evidence that this surface reconstruction has a low dipole moment, which makes it significantly more stable than either of the pure KO or TaO_2 terminations. This observation is reminiscent of the partial SrO termination proposed in the present work for the LSM25(001) surface. While we cannot say for certain that the findings by Setvin *et al.* will be equally applicable to LSM25, we find this experimental finding encouraging because it shows that such mixed terminations can be stable, despite the fact that they have a higher density of undercoordinated sites than the perfect terminations.

One of the major differences to $KTaO_3$ is that LSM25 is a doped system, from which different behavior may arise. In fact, in the case of LSM25, we find that the partial SrO termination has a lower surface free energy than the partial LaO termination in the studied range of temperature and $p(O_2)$. This is the result of the higher chemical potential of the Sr dopant compared to the La host cation. Furthermore, due to the favorable electrostatic interaction between the positively charged SrO surface domains with the negatively charged Sr dopants below the surface, the location where SrO domains appear on the surface may be controlled by the location of Sr dopant cations. This suggests that the SrO domains may not order on the surface in the way it is observed for $KTaO_3$. This idea is further supported by our observation that many different surface configurations are within a narrow range of surface free energies in Fig. 4. Based on these considerations, we expect the surface termination in LSM25 to be disordered, in contrast to the $KTaO_3(001)$ labyrinth reconstruction. Unfortunately, a potential disorder of the surface termination cannot be modeled in a DFT-based super cell approach as applied in the present manuscript. Monte Carlo simulations to study disorder on the LSM25 surface may be the subject of future work. These differences between $KTaO_3$ and LSM25 highlight how greatly the behavior of the dopant cation can differ from the host cation, which is one of the factors that govern the segregation of dopant cations to the surface.

Our model predicts a 50%-covering SrO termination to be the stable termination over a large range of T and $p(O_2)$ under slightly reducing conditions. Although we are certain that the error due to approximating the cation chemical potentials as constant is sizeable, the surface is likely to expose both MnO_2 and (La,Sr)O domains under SOFC conditions: $[\,V_O^{\cdot\cdot} - V_A^{'''}]$ defects are cheap in terms of energy (1.85 eV, −0.17 eV [sic], and 0.90 eV at 0 K at the MnO_2, LaO and SrO terminations, respectively) and are expected to have concentrations in the percent range at elevated temperatures.

D. Possible role of the partial SrO and LaO terminations in the oxygen reduction reaction

Since the partial SrO termination is expected to dominate the surface under SOFC operating conditions, we examine its possible relevance in the oxygen reduction reaction. For assessing the catalytic activity of SOFC cathodes in the oxygen reduction reaction (ORR), several different factors play a role, such as the coverage of adsorbed oxygen and its dissociation barrier, but also the oxygen vacancy concentration near the surface and the mobility of these vacancies [17,29,34–36]. While we have not studied these aspects yet in detail for our proposed partial MnO_2/LaO/SrO terminations, we would like to point out that such terminations may have special properties in the context of the ORR, based on the results of previous studies of Merkle *et al.* [33] and Mastrivkov *et al.* [29]. Mastrikov *et al.* studied in detail the formation and occupation of important intermediates in the ORR (surface oxygen vacancies and adsorbed oxygen) for the different terminations [MnO_2 and (La,Sr)O] of LSM50(001) [29]. Finally, they note that each of these polar terminations favor intermediates of opposing charge ($V_O^{\cdot\cdot}$ at MnO_2, $O_{2,ad}^-$ on LaO), which results in a high coverage of the surface with the favored intermediate and very little of the other [29]. This means that the MnO_2 termination will have many oxygen vacancies, but little adsorbed oxygen, and the LaO termination will have a lot of adsorbed oxygen, but few oxygen vacancies [29]. Mastrikov *et al.* concluded that the recombination of adsorbed oxygen with a surface oxygen vacancy should be rate-determining [29] based on energetics of reaction intermediates.

In the present manuscript, we propose a mixed surface termination that is overall unpolar, but consists of positively charged SrO domains in close proximity to negatively charged MnO_2 domains. If the LSM25 surface under SOFC operating conditions is indeed patterned this way, the boundary between the (La,Sr)O and MnO_2 domains may be the active site where adsorbed oxygen recombines with surface oxygen vacancies. Due to the lower positive surface charge of SrO domains compared to LaO domains, we expect $O_{2,ad}^-$ to bind less strongly to SrO than to LaO. We therefore propose that a catalytically active surface requires LaO domains, while the partial SrO termination proposed for the equilibrated surface represents a deactivated or degraded state where O_2 does not

adsorb as strongly. While we cannot be certain that this is the case at present, we propose to include associated [$V_{O}^{\cdot\cdot}$ − $V_{cation}^{\prime\prime\prime}$] defects and patterned partial terminations in the future discussion of the active center in the ORR.

V. SUMMARY AND CONCLUSION

We have examined the effect of $p(O_2)$ and temperature on Sr segregation at the LSM25(001) surface by an *ab initio* thermodynamics model. It takes into account different terminations and surface reconstructions of the LSM25(001) surface, point defects $Sr_{La}^{\prime}$, $V_{O}^{\cdot\cdot}$, $V_{Mn}^{\prime\prime\prime}$, $V_{La}^{\prime\prime\prime}$, O_{ad} near the surface and at the surface terminations, as well as associated point defects of the type [$V_{O}^{\cdot\cdot}$ − $V_{cation}^{\prime\prime\prime}$] and [$V_{O}^{\cdot\cdot}$ − $Sr_{La}^{\prime}$], and their influence on the relative stabilities of surface terminations.

This is the first computational model of the LSM25(001) surface that takes into account how surface defects influence the stabilities of surface terminations. As a result, this model is able to make quantitative predictions about the Sr surface enrichment as a function of (T, $p(O_2)$) and the factors that drive changes in the surface composition. This was achieved by explicitly computing cation chemical potentials in the bulk and considering a large number of possible surface structures with a variety of (coexisting) defects at the different terminations and combining them in an *ab initio* thermodynamics model.

Our results show that the MnO_2 termination is preferred under oxidizing conditions, while a partially covering SrO termination on MnO_2 becomes stable already at 1100 K at 0.2 bar O_2 and remains stable over a wide range of more reducing conditions. This change is driven by the reduction of the surface dipole density upon partially covering the negatively charged MnO_2 surface by positively charged SrO domains. The average surface composition is computed quantitatively by considering not only the surface structure that minimizes the Gibbs free energy, but an average over the convex hull as a function of, for instance, the near-surface Sr content. This calculation shows that Sr is enriched close to the surface under reducing conditions, which is a direct consequence of the increased formation of positively charged oxygen vacancies at the surface. These vacancies are formed due to the reduction of the oxygen chemical potential and stabilize Sr near the surface and vice versa, resulting in the observed near-surface Sr enrichment as the gas phase becomes more reducing. This trend is found for all the considered surface terminations because the Sr enrichment at the surface is purely driven by electrostatic interaction between the positively charged oxygen vacancies and the negatively charged Sr dopant. Therefore, this conclusion is likely valid for other facets of LSM, as well as other nonstoichiometric perovskite oxides.

We propose a new termination of the LSM25(001) surface at reducing conditions; that is the partial SrO termination, which consists of a SrO layer that covers the underlying MnO_2 only partially and leaves both Mn and O sites of the MnO_2 layer exposed. Both positively and negatively charged surfaces appear to be essential for the stabilization of charged intermediates in the oxygen reduction reaction [29]. While each of the perfect terminations, MnO_2 and (La,Sr)O exposes only one type of polarity (negative or positive), a partially covering termination exposes both positive and negative MnO_2 and (La,Sr)O domains in close proximity while being overall neutral. Because such partially covering terminations and associated cation vacancy-oxygen vacancy clusters solve the fundamental polarity problem of the perovskite (001) surface, we propose including them in the future discussion of the active site in the ORR.

ACKNOWLEDGMENTS

We thank the German Research Foundation (DFG) for a postdoc fellowship for Franziska Hess (Project No. 324830457) and the MIT Energy Initiative for supplementary funding. This project would not have been possible without the computation time allocated by XSEDE (Grant No. TG-DMR120025) and NERSC (Contract No. DE-AC02-05CH11231) on the Stampede2 and Cori high performance computing clusters. We gratefully acknowledge the staff at TACC, NERSC, and MGHPCC for technical support.

[1] H. Zhu, P. Zhang, and S. Dai, Recent advances of lanthanum-based perovskite oxides for catalysis, ACS Catalysis **5**, 6370 (2015).

[2] J. Hwang, R. R. Rao, L. Giordano, Y. Katayama, Y. Yu, and Y. Shao-Horn, Perovskites in catalysis and electrocatalysis, Science **358**, 751 (2017).

[3] F. Polo-Garzon and Z. Wu, Acid–base catalysis over perovskites: A review, J. Mater. Chem. A **6**, 2877 (2018).

[4] C. Rao and S. Dey, Generation of H_2 and CO by solar thermochemical splitting of H_2O and CO_2 by employing metal oxides, J. Solid State Chem. **242**, 107 (2016).

[5] C. Agrafiotis, M. Roeb, and C. Sattler, A review on solar thermal syngas production via redox pair-based water/carbon dioxide splitting thermochemical cycles, Renewable Sustainable Energy Rev. **42**, 254 (2015).

[6] J. Scheffe and A. Steinfeld, Oxygen exchange materials for solar thermochemical splitting of H_2O and CO_2: A review, Mater. Today **17**, 341 (2014).

[7] L. Malavasi, C. A. J. Fisher, and M. S. Islam, Oxide-ion and proton conducting electrolyte materials for clean energy applications: Structural and mechanistic features, Chem. Soc. Rev. **39**, 4370 (2010).

[8] E. de Souza and R. Muccillo, Properties and applications of perovskite proton conductors, Mater. Res. **13**, 385 (2010).

[9] B. Han, M. Risch, Y.-L. Lee, C. Ling, H. Jia, and Y. Shao-Horn, Activity and stability trends of perovskite oxides for oxygen evolution catalysis at neutral pH, Phys. Chem. Chem. Phys. **17**, 22576 (2015).

[10] Z. Feng, W. T. Hong, D. D. Fong, Y.-L. Lee, Y. Yacoby, D. Morgan, and Y. Shao-Horn, Catalytic activity and stability of oxides: The role of near-surface atomic structures and compositions, Acc. Chem. Res. **49**, 966 (2016).

[11] A. van Roekeghem, J. Carrete, C. Oses, S. Curtarolo, and N. Mingo, High-Throughput Computation of Thermal Conductivity of High-Temperature Solid Phases: The Case of Oxide and Fluoride Perovskites, Phys. Rev. X **6**, 041061 (2016).

[12] Y. M. Sheu, S. A. Trugman, L. Yan, J. Qi, Q. X. Jia, A. J. Taylor, and R. P. Prasankumar, Polaronic Transport Induced by Competing Interfacial Magnetic Order in a $La_{0.7}Ca_{0.3}MnO_3/BiFeO_3$ Heterostructure, Phys. Rev. X **4**, 021001 (2014).

[13] P. A. Kumar, R. Mathieu, P. Nordblad, S. Ray, O. Karis, G. Andersson, and D. D. Sarma, Reentrant Superspin Glass Phase in a $La_{0.82}Ca_{0.18}MnO_3$ Ferromagnetic Insulator, Phys. Rev. X **4**, 011037 (2014).

[14] P. Moetakef, J. R. Williams, D. G. Ouellette, A. P. Kajdos, D. Goldhaber-Gordon, S. J. Allen, and S. Stemmer, Carrier-Controlled Ferromagnetism in $SrTiO_3$, Phys. Rev. X **2**, 021014 (2012).

[15] G. Cheng *et al.*, Anomalous Transport in Sketched Nanostructures at the $LaAlO_3/SrTiO_3$ Interface, Phys. Rev. X **3**, 011021 (2013).

[16] Z. Zhong and P. Hansmann, Band Alignment and Charge Transfer in Complex Oxide Interfaces, Phys. Rev. X **7**, 011023 (2017).

[17] F. Hess, A. Staykov, B. Yildiz, and J. Kilner, Solid oxide fuel cell materials and interfaces, *Handbook of Materials Modeling* (Springer, Cham, 2019).

[18] X. Cheng, E. Fabbri, Y. Yamashita, I. E. Castelli, B. Kim, M. Uchida, R. Haumont, I. Puente-Orench, and T. J. Schmidt, Oxygen evolution reaction on perovskites: A multieffect descriptor study combining experimental and theoretical methods, ACS Catalysis **8**, 9567 (2018).

[19] J. Suntivich, K. J. May, H. A. Gasteiger, J. B. Goodenough, and Y. Shao-Horn, A perovskite oxide optimized for oxygen evolution catalysis from molecular orbital principles, Science **334**, 1383 (2011).

[20] J. Suntivich, H. Gasteiger, N. Yabuuchi, H. Nakanishi, J. Goodenough, and Y. Shao-Horn, Design principles for oxygen-reduction activity on perovskite oxide catalysts for fuel cells and metal–air batteries, Nat. Chem. **3**, 546 (2011).

[21] Y. Li, W. Zhang, Y. Zheng, J. Chen, B. Yu, Y. Chen, and M. Liu, Controlling cation segregation in perovskite-based electrodes for high electro-catalytic activity and durability, Chem. Soc. Rev. **46**, 6345 (2017).

[22] B. Koo, K. Kim, J. Kim, H. Kwon, J. Han, and W. Jung, Sr segregation in perovskite oxides: Why it happens and how it exists, Joule **2**, 1476 (2018).

[23] Y. Chen, W. Jung, Z. Cai, J. Kim, H. Tuller, and B. Yildiz, Impact of Sr segregation on the electronic structure and oxygen reduction activity of $SrTi_{1-x}Fe_xO_3$ surfaces, Energy Environ. Sci. **5**, 7979 (2012).

[24] W. Lee, J. Han, Y. Chen, Z. Cai, and B. Yildiz, Cation size mismatch and charge interactions drive dopant segregation at the surfaces of manganite perovskites, J. Am. Chem. Soc. **135**, 7909 (2013).

[25] W. Lee and B. Yildiz, Factors that influence cation segregation at the surfaces of perovskite oxides, ECS Trans. **57**, 2115 (2013).

[26] N. Tsvetkov, Q. Lu, L. Sun, E. Crumlin, and B. Yildiz, Improved chemical and electrochemical stability of perovskite oxides with less reducible cations at the surface, Nat. Mater. **15**, 1010 (2016).

[27] Y. Chen, H. Tellez, M. Burriel, F. Yang, N. Tsvetkov, Z. Cai, D. McCombd, J. Kilner, and B. Yildiz, Segregated chemistry and structure on (001) and (100) surfaces of $(La_{1-x}Sr_x)_2CoO_4$ override the crystal anisotropy in oxygen exchange kinetics, Chem. Mater **27**, 5436 (2015).

[28] Z. Cai, M. Kubicek, J. Fleig, and B. Yildiz, Chemical heterogeneities on $La_{0.6}Sr_0.4CoO_{3-\delta}$ thin films–correlations to cathode surface activity and stability, Chem. Mater **24**, 1116 (2012).

[29] Y. A. Mastrikov, R. Merkle, E. A. Kotomin, M. Kuklja, and J. Maier, Surface termination effects on the oxygen reduction reaction rate at fuel cell cathodes, J. Mater. Chem. A **6**, 11929 (2018).

[30] M. Gadre, Y.-L. Lee, Y. Shao-Horn, and D. Morgan, Catalytic activity of (001)-AO and BO_2 surfaces of transition metal perovskites: The case of $LaCrO_3$, ECS Trans. **58**, 1 (2014).

[31] M. M. Kuklja, E. A. Kotomin, R. Merkle, Y. A. Mastrikov, and J. Maier, Combined theoretical and experimental analysis of processes determining cathode performance in solid oxide fuel cells, Phys. Chem. Chem. Phys. **15**, 5443 (2013).

[32] Y. Wang and H.-P. Cheng, Oxygen reduction activity on perovskite oxide surfaces: A comparative first-principles study of $LaMnO_3$, $LaFeO_3$, and $LaCrO_3$, J. Phys. Chem. C **117**, 2106 (2013).

[33] R. Merkle, Y. Mastrikov, E. Heifets, E. Kotomin, M. Kukla, and J. Maier, Oxygen incorporation reaction into mixed conducting perovskites: A mechanistic analysis for (La, Sr)MnO_3 based on DFT calculations, ECS Trans. **25**, 2753 (2009).

[34] T. Akbay, A. Staykov, J. Druce, H. Téllez, T. Ishihara, and J. A. Kilner, The interaction of molecular oxygen on LaO terminated surfaces of La_2NiO_4, J. Mater. Chem. A **4**, 13113 (2016).

[35] A. Staykov, H. Téllez, T. Akbay, J. Druce, T. Ishihara, and J. Kilner, Oxygen activation and dissociation on transition metal free perovskite surfaces, Chem. Mater. **27**, 8273 (2015).

[36] A. Staykov, H. Téllez, J. Druce, J. Wu, T. Ishihara, and J. Kilner, Electronic properties and surface reactivity of SrO-terminated $SrTiO_3$ and SrO-terminated iron-doped $SrTiO_3$, Sci. Technol. Adv. Mater. **19**, 221 (2018).

[37] M. Riva *et al.*, Influence of surface atomic structure demonstrated on oxygen incorporation mechanism at a model perovskite oxide, Nat. Commun. **9**, 3710 (2018).

[38] A.-K. Huber, M. Falk, M. Rohnke, B. Luerssen, M. Amati, L. Gregoratti, D. Hesse, and J. Janek, In situ study of activation and de-activation of LSM fuel cell cathodes–Electrochemistry and surface analysis of thin-film electrodes, J. Catal. **294**, 79 (2012).

[39] T. T. Fister, D. D. Fong, J. A. Eastman, P. M. Baldo, M. J. Highland, P. H. Fuoss, K. R. Balasubramaniam, J. C. Meador, and P. A. Salvador, In situ characterization of strontium surface segregation in epitaxial $La_{0.7}Sr_{0.3}MnO_3$ thin films as a function of oxygen partial pressure, Appl. Phys. Lett. **93**, 151904 (2008).

[40] J. Druce, H. Téllez, M. Burriel, M. Sharp, L. Fawcett, S. Cook, D. McPhail, T. Ishihara, H. Brongersma, and J. Kilner, Surface termination and subsurface restructuring of perovskite-based solid oxide electrode materials, Energy Environ. Sci. **7**, 3593 (2014).

[41] J. Y. Koo, H. Kwon, M. Ahn, M. Choi, J.-W. Son, J. W. Han, and W. Lee, Suppression of cation segregation in (La, Sr)$CoO_{3-\delta}$ by elastic energy minimization, ACS Appl. Mater. Interfaces **10**, 8057 (2018).

[42] Y.-L. Lee and D. Morgan, *Ab initio* defect energetics of perovskite (001) surfaces for solid oxide fuel cells: A comparative study of $LaMnO_3$ versus $SrTiO_3$ and $LaAlO_3$, Phys. Rev. B **91**, 195430 (2015).

[43] S. Jiang, Development of lanthanum strontium manganite perovskite cathode materials of solid oxide fuel cells: A review, J. Mater. Sci. **43**, 6799 (2008).

[44] W. Wang and S. Jiang, A mechanistic study on the activation process of (La, Sr)MnO_3 electrodes of solid oxide fuel cells, Solid State Ion. **177**, 1361 (2006).

[45] D. Kim, R. Bliem, F. Hess, J.-J. Gallet, and B. Yildiz, Electrochemical polarization dependence of the elastic and electrostatic driving forces to aliovalent dopant segregation on $LaMnO_3$, J. Am. Chem. Soc. (2020), doi: 10.1021/jacs.9b13040.

[46] H. Kwon, W. Lee, and J. W. Han, Suppressing cation segregation on lanthanum-based perovskite oxides to enhance the stability of solid oxide fuel cell cathodes, RSC Adv. **6**, 69782 (2016).

[47] P. Tasker, The stability of ionic crystal surfaces, J. Phys. C: Solid State Phys. **12**, 4977 (1979).

[48] N. Nakagawa, H. Hwang, and D. Muller, Why some interfaces cannot be sharp, Nat. Mater. **5**, 204 (2006).

[49] J. Goniakowski and C. Noguera, The concept of weak polarity: an application to the $SrTiO_3(001)$ surface, Surf. Sci. Lett. **365**, L657 (1996).

[50] W. Harrison, Origin of Sr segregation at $La_{1-x}Sr_xMnO_3$ surfaces, Phys. Rev. B **83**, 155437 (2011).

[51] E. J. Crumlin, E. Mutoro, Z. Liu, M. E. Grass, M. D. Biegalski, Y.-L. Lee, D. Morgan, H. M. Christen, H. Bluhm, and Y. Shao-Horn, Surface strontium enrichment on highly active perovskites for oxygen electrocatalysis in solid oxide fuel cells, Energy Environ. Sci. **5**, 6081 (2012).

[52] Q. Lu, G. Vardar, M. Jansen, S. R. Bishop, I. Waluyo, H. L. Tuller, and B. Yildiz, Surface defect chemistry and electronic structure of $Pr_{0.1}Ce_{0.9}O_{2-\delta}$ revealed in operando, Chem. Mater. **30**, 2600 (2018).

[53] X. Guo and R. Waser, Space charge concept for acceptor-doped zirconia and ceria and experimental evidences, Solid State Ion. **173**, 63 (2004).

[54] W. C. Chueh, A. H. McDaniel, M. E. Grass, Y. Hao, N. Jabeen, Z. Liu, S. M. Haile, K. F. McCarty, H. Bluhm, and F. El Gabaly, Highly enhanced concentration and stability of reactive Ce^{3+} on doped CeO_2 surface revealed in operando, Chem. Mater. **24**, 1876 (2012).

[55] A. F. Zurhelle, X. Tong, A. Klein, D. S. Mebane, and R. A. De Souza, A space-charge treatment of the increased concentration of reactive species at the surface of a ceria solid solution, Angew. Chem. Int. Ed. **56**, 14516 (2017).

[56] Z. Zhao, M. Uddi, N. Tsvetkov, B. Yildiz, and A. F. Ghoniem, Redox kinetics study of fuel reduced ceria for chemical-looping water splitting, J. Phys. Chem. C **120**, 16271 (2016).

[57] L. Sun, D. Marrocchelli, and B. Yildiz, Edge dislocation slows down oxide ion diffusion in doped CeO_2 by segregation of charged defects, Nat. Comm. **6**, 6294 (2015).

[58] J. Yang, M. Youssef, and B. Yildiz, Predicting point defect equilibria across oxide hetero-interfaces: model system of ZrO_2/Cr_2O_3, Phys. Chem. Chem. Phys. **19**, 3869 (2017).

[59] M. Reticcioli, M. Setvin, X. Hao, P. Flauger, G. Kresse, M. Schmid, U. Diebold, and C. Franchini, Polaron-Driven Surface Reconstructions, Phys. Rev. X **7**, 031053 (2017).

[60] V. Sharma, M. Mahapatra, P. Singh, and R. Ramprasad, Cationic surface segregation in doped $LaMnO_3$, J. Mater. Sci. **50**, 3051 (2015).

[61] S. Piskunov, E. Heifets, T. Jacob, E. Kotomin, D. Ellis, and E. Spohr, Electronic structure and thermodynamic stability of $LaMnO_3$ and $La_{1-x}Sr_xMnO_3(001)$ surfaces: *Ab initio* calculations, Phys. Rev. B **78**, 121406 (2008).

[62] Y.-L. Lee and D. Morgan, *Ab initio* and empirical defect modeling of $LaMnO_{3\pm\delta}$ for solid oxide fuel cell cathodes, Phys. Chem. Chem. Phys. **14**, 290 (2012).

[63] S. Gerhold, Z. Wang, M. Schmid, and U. Diebold, Stoichiometry-driven switching between surface reconstructions on $SrTiO_3(001)$, Surf. Sci. **621**, L1 (2014).

[64] J. M. P. Martirez, S. Kim, E. H. Morales, B. T. Diroll, M. Cargnello, T. R. Gordon, C. B. Murray, D. A. Bonnell, and A. M. Rappe, Synergistic oxygen evolving activity of a TiO_2- rich reconstructed $SrTiO_3(001)$ surface, J. Am. Chem. Soc. **137**, 2939 (2015).

[65] N. Erdman, K. Poeppelmeier, M. Asta, O. Warschkow, D. Ellis, and L. Marks, The structure and chemistry of the TiO_2- rich surface of $SrTiO_3(001)$, Nature **419**, 55 (2002).

[66] S. Cook and L. Marks, *Ab initio* predictions of double-layer TiO_2- terminated $SrTiO_3(001)$ surface reconstructions, J. Phys. Chem. C **122**, 21991 (2018).

[67] M. Setvin, M. Reticcioli, F. Poelzleitner, J. Hulva, M. Schmid, L. A. Boatner, C. Franchini, and U. Diebold, Polarity compensation mechanisms on the perovskite surface $KTaO_3(001)$, Science **359**, 572 (2018).

[68] J. Druce, T. Ishihara, and J. Kilner, Surface composition of perovskite-type materials studied by Low Energy Ion Scattering (LEIS), Solid State Ion. **262**, 893 (2014).

[69] H. Téllez, J. Druce, Y. Shi, N. S. M. Kubicek and, J. Rupp, T. Ishihara, and J. Kilner, Surface segregation and inter-diffusion of cations and impurities in microelectrodes for solid oxide fuel cells and electrolysers, ECS Trans. **66**, 69 (2015).

[70] S. V. Merzlikin, N. N. Tolkachev, L. E. Briand, T. Strunskus, C. Wöll, I. E. Wachs, and W. Grünert, Anomalous surface compositions of stoichiometric mixed oxide compounds, Angew. Chem. Int. Ed. **49**, 8037 (2010).

[71] G. Kresse and J. Furthmüller, Efficient iterative schemes for *ab initio* total-energy calculations using a plane-wave basis set, Phys. Rev. B **54**, 11169 (1996).

[72] G. Kresse and D. Joubert, From ultrasoft pseudopotentials to the projector augmented-wave method, Phys. Rev. B **59**, 1758 (1999).

[73] J. P. Perdew, J. A. Chevary, S. H. Vosko, K. A. Jackson, M. R. Pederson, D. J. Singh, and C. Fiolhais, Atoms, molecules, solids, and surfaces: Applications of the generalized gradient approximation for exchange and correlation, Phys. Rev. B **46**, 6671 (1992).

[74] S. L. Dudarev, G. A. Botton, S. Y. Savrasov, C. J. Humphreys, and A. P. Sutton, Electron-energy-loss spectra and the structural stability of nickel oxide: An LSDA+U study, Phys. Rev. B **57**, 1505 (1998).

[75] L. Wang, T. Maxisch, and G. Ceder, Oxidation energies of transition metal oxides within the GGA+U framework, Phys. Rev. B **73**, 195107 (2006).

[76] J. Rodriguez-Carvajal, M. Hennion, F. Moussa, A. H. Moudden, L. Pinsard, and A. Revcolevschi, Neutron-diffraction study of the Jahn-Teller transition in stoichiometric $LaMnO_3$, Phys. Rev. B **57**, R3189 (1998).

[77] See Supplemental Material at http://link.aps.org/supplemental/10.1103/PhysRevMaterials.4.015801 for details on the oxygen

defect chemistry of LSM; quantitative comparison of cation chemical potentials with different references; an interactive applet to display surface energies, near-surface Sr content, near-surface oxygen content and surface dipole moment as a function of (T, $p(O_2)$); the Bader charge analysis; an estimate of μ_{Sr} as a function of (T, $p(O_2)$); and more detailed information on the interplay of surface polarity and near-surface Sr enrichment.

[78] B. Dabrowski *et al.*, Structure-properties phase diagram for $La_{1-x}Sr_xMnO_3$ ($0.1 < x < 0.2$), Phys. Rev. B **60**, 7006 (1999).

[79] S. Xu, Y. Moritomo, K. Ohoyama, and A. Nakamura, Neutron structural analysis of $La_{1-x}Sr_xMnO_3$–variation of one-electron bandwidth W with hole doping, J. Phys. Soc. Japan **72**, 709 (2003).

[80] L. Pinsard, J. Rodriguez-Carvajal, and A. Revcolevschi, Structural phase diagram of $La_{1-x}Sr_xMnO_3$ for low Sr doping, J. Alloy Compd. **262–263**, 152 (1997).

[81] J. Mitchell, D. Argyriou, C. Potter, D. Hinks, J. Jorgensen, and S. Bader, Structural phase diagram of $La_{1-x}Sr_xMnO_{3+\delta}$: Relationship to magnetic and transport properties, Phys. Rev. B **54**, 6172 (1996).

[82] J. Nowotny and M. Rekas, Defect chemistry of (La, Sr)MnO_3, J. Am. Ceram Soc. **81**, 67 (1998).

[83] NIST chemistry webbook, https://webbook.nist.gov/chemistry/.

[84] P. Ewald, Die Berechnung optischer und elektrostatischer Gitterpotentiale, Ann. Phys. **369**, 253 (1921).

[85] K. Kuroda, N. Ishizawa, N. Mizutani, and M. Kato, The crystal structure of α-$SrMnO_3$, J. Solid State Chem. **38**, 297 (1981).

[86] P. Battle, T. Gibb, and C. Jones, The structural and magnetic properties of $SrMnO_3$: A reinvestigation, J. Solid State Chem. **74**, 60 (1988).

[87] J. Mizusaki *et al.*, Oxygen nonstoichiometry and defect equilibrium in the perovskite-type oxides $La_{1-x}Sr_xMnO_{3+\delta}$, Solid State Ion. **129**, 163 (2000).

[88] J. Kuo, H. Anderson, and D. Sparlin, Oxidation-reduction behavior of undoped and Sr-doped $LaMnO_3$ nonstoichiometry and defect structure, J. Solid State Chem. **83**, 52 (1989).

[89] T. C. Leung, C. L. Kao, W. S. Su, Y. J. Feng, and C. T. Chang, Relationship between surface dipole, work function and charge transfer: Some exceptions to an established rule, Phys. Rev. B **68**, 195408 (2003).